Report on the model application to evaluate the efficiency of migration strategies for the selected scenarios of climate changes

Deliverable D_3.4.5

Contributing partners:

LP – UNIPD DICEA

PP4 – UNIST-FGAG

PP5 – CROATIAN WATERS

PP6 – DUNEA

Section 1

The Italian site 1/2: the pipe drain scale

TABLE OF CONTENTS

1. Introduction and research questions: preliminary pipe drain analysis

The Canal Morto is supposed to supply fresh water to the soil in order to contrast the saltwater intrusion. A drain is installed into the soil to facilitate the distribution of the fresh water of the Canal Morto to the area and prevent saltwater contamination of the crops. The relationship between the Canal Morto water levels and the freshwater discharge provided through the drain needs to be estimated in order to design and verify the drain countermeasure

2. Study area: physical reality

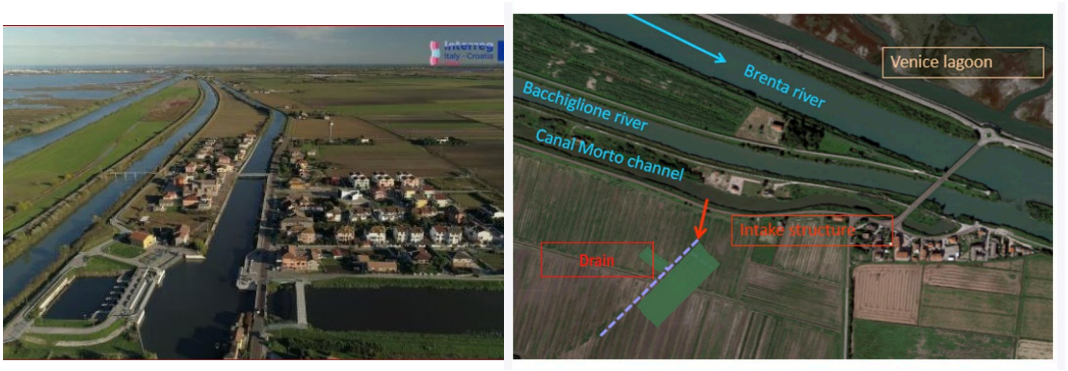

Figure 1: 3d plot and plan view of the study area. The Brenta and Bacchiglione rivers together with the Canal Morto Channel can be seen as well as the location of the pipe drain.

The case study area is located 5 near Ca' Pasqua locality, Chioggia municipality, in the southern part of Venice lagoon, in the north-west side of Pianura Padana. The study area is complex due to the interplay of different physical elements: the Bacchiglione and Brenta rivers cross the study area just before flowing into the Adriatic Sea; the Morto channel, whose water level is controlled by a lock gate system, collecting reclamation waters by an upstream pumping station, flows inside the study area, parallel to the Bacchiglione river, while the Venice lagoon lies in the north-east boundary of the domain and in the south-west side there are mainly agricultural fields, characterized by the presence of slum areas and barene, which evolve until Bocca di Chioggia. In the west boundary there are mainly agriculture fields. The depth of the top of the plume (that corresponds to the interface between freshwater and saltwater) is spatially very variable and in some areas it touches the soil surface. The

depth of the top of the intrusion depends on hydraulic and meteorological conditions and the fluctuations are more evident in the first 10 m of subsoil; the freshwater/saltwater interface varies from 2 to 30 m below the ground level, depending strongly on seasonal variations. The average of the bottom of the plume, generally, is 10-15 m for the Northernmost zone and it reaches even 100 m in depth in the subsoil in the Southernmost zone of the area. The subsoil reports a complex stratigraphy. It's possible to define schematically the layers' composition of the soil, which consists of three main soil types: basematerial, sand and limosilt. From -3 m (a.s.l) in depth to -11.8 m (a.s.l) in depth are present some sandy bodies, which are the remains of ancient littorals ridges and paleo-channels from Late Pleistocene and Holocene. The sandy bodies have a higher hydraulic conductibility in comparison with the surrounding soil, and this entails a faster penetration of the saline intrusion in the mentioned zones. Inside the paleochannels, at about -0.5 m underground (a.s.l), there is coarse sand, till about -11.8 underground (a.s.l); in the remaining area the soil is composed primarily of shells, silt and fine sand. At about -18 m (a.s.l), it's present a caranto unit (an over-consolidated clay layer, that separates the Holocene from the Pleistocene deposits), which, with its low conductivity, acts as a natural barrier and prevents a deeper propagation of saltwater and saline intrusion downward. The aquifer inside the study area is a phreatic shallow one and it's the most superficial part of a complex multi-pitch system of aquifers, which characterize the Venetian area.

3. Models

3.1 Conceptual model

The conceptual model consists of a reservoir of level H1which provides fresh water to the fields through a drain (L1+L2), given the head difference (H1-H2). The water head – blue line - is described in the following plot. Note that the distributing part of the drain is located in the first part of the manufacture, L_1, while the draining part is related to the second part, L_2.

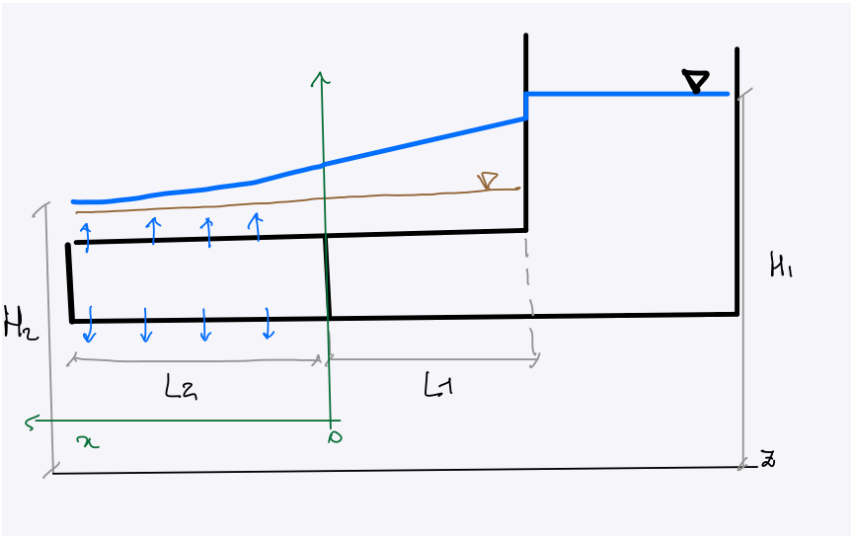

Figure 2: Conceptual hydraulic model

3.2 Model equations and assumptions

The following system of equations represents the freshwater head function given the losses - local - at the reservoir, $K_i \frac{v_1^2}{2g}$, where K_i is a local loss coefficient, v_1 is the velocity - and distributed (linear and quadratic) at the drian, with j_1 and j_2 are the slope coefficients of the drain. $q = \frac{Q}{L}$ is the discharge per unit length equation, describing the quantity of freshwater is provided to the domain, where $C_q \varepsilon$ are coefficients describing the drainage characteristics of the drain whilst the term $h(x) - H_2$ describing the head difference represents the acting force on the system allowing the discharge to flow.

$$\begin{cases} h(x) = H_1 - \left\{\left[K_i \frac{v_1^2}{2g} + L_1 j_1\right] + \left[\int_0^x j_2 dx\right]\right\} \\ q = \frac{Q}{L} = C_q \varepsilon \sqrt{2g(h(x) - H_2)} \end{cases} \quad \text{Eq. 1}$$

In reality, the ditches drain variably salted water from the inland, whereas the pipe drain provide fresh water from the Morto Channel to the domain.

Note that the equations system is an implicit system of equations which cannot be solved directly. Moreover, the drain at Ca' Pasqua site is surrounded by soil to provide freshwater to the ground soil contrasting the saltwater intrusion. This means the infiltration of freshwater to the ground soil is described by the Darcy's law dynamics so that the system becomes

$$\begin{cases} h(x) = H_1 - \left\{\left[K_i \frac{v_1^2}{2g} + L_1 j_1\right] + \left[\int_0^x j_2 dx\right]\right\} \\ q = \frac{Q}{L} = v_2 \Phi \pi = \left(\frac{K \Phi \pi}{d}\right) \Delta H \end{cases} \quad \text{Eq. 2}$$

K is the hydraulic conductivity of the soil, Φ, d are the ray of the circular area of the drain and the diameter respectively, and ΔH is the head difference moving the freshwater to the soil.

4. Numerical model

Once the physical and conceptual models have been set-up, a number of numerical simulations are performed to quantify how much freshwater is provided given different head and hydraulic conductivity conditions. Each scenario will be briefly described in the following together with a description of the main founding at the end of the report.

4.1 Main characteristics

A 2D cross section domain is used for the numerical simulations. The area is located between two ditches and it is axial symmetric so that just half of the whole domain is considered in the simulations (Feflow environment).

DITCH: Depth equal to 1 m

PIPE DRAIN: diameter 0.16 m

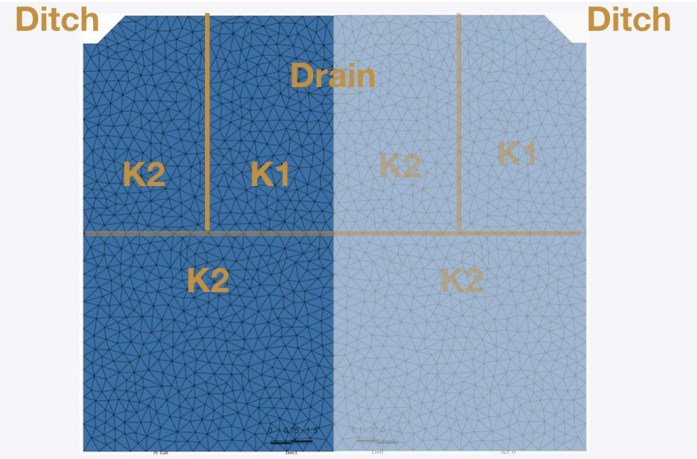

Figure 3:axial Symmetric numerical model mesh

Geometry and stratigraphy

K_1 and K_2 stand for two different type of soils. Model stratigraphy reports a fine sandy area representing the paleo-channels where the pipe drain is supposed to be located to take advantage of the higher value of hydraulic conductivity, while the rest of the model is characterized by base – material. Model parametrization is reported in the following

Time resolution and Data availability

SIMULATION time_ 4 years

COMPUTATIONAL time= 1 minute

4.2 Numerical simulations

Simulations have been run in the Feflow environment which allows the applications of the Richards' equations in steady and transient conditions. The 2D models presents axial symmetry which implies a no flux conditions along the symmetry axis and Dirichlet boundary conditions both for the pipe drain and for the ditches. Different hydraulic conductivity values are considered, and the Van Genuchten water retention curves are applied for the vadose zone (note that the area devoted to the unsatured dynamics is very small, this is the reason why the same water retention curve is applied for both the soils). More details are provided in the following sections.

Table 1:Mesh characteristics

Element type	Triangle
Mesh elements	1572
Mesh nodes	833
Area	139.4 m2

Table 2:Initial and boundary conditions

Boundary Conditions	**DRAINING DITCH:** Dirichlet fixed head boundary condition equal to -0.5 m from the soil **PIPE DRAIN:** Dirichlet boundary conditions. Three different pipe drain scenarios are considered (the head is applied to the 5 nodes representing the drain) H0= 0 m from the soil H1=-+1 m from the soil H2=+ 2 m from the soil Values are kept fixed in time
Initial Conditions	**WATER TABLE POSITION:** -0.5m from the soil
Hydraulic Conductivity	See following tables
Specific storage	See following tables
Porosity	See following tables

Van Genuchten parameters	See following tables

Table 3: model parameters

	Base material	**Sand**
Kx=Ky=Kz (reference values – to be changed in the simulations)	32.64[m/d] = 3.77 10^-4 [m/s]	326.4[m/d] = 3.77 10^-3[m/s]
anisotropy	3	3
Ss [1/m]	0.00001	0.00001
Theta_s=porosity	0.3	0.3
Theta_r	0	0
ss	1	1
Alfa[1/m]	5.5[1/m] = 5.61 10^-4 [1/Pa]	5.5[1/m] = 5.61 10^-4 [1/Pa]
n	2.8	2.8

Vadose zone water retention curves (for Van Genuchten parameters)

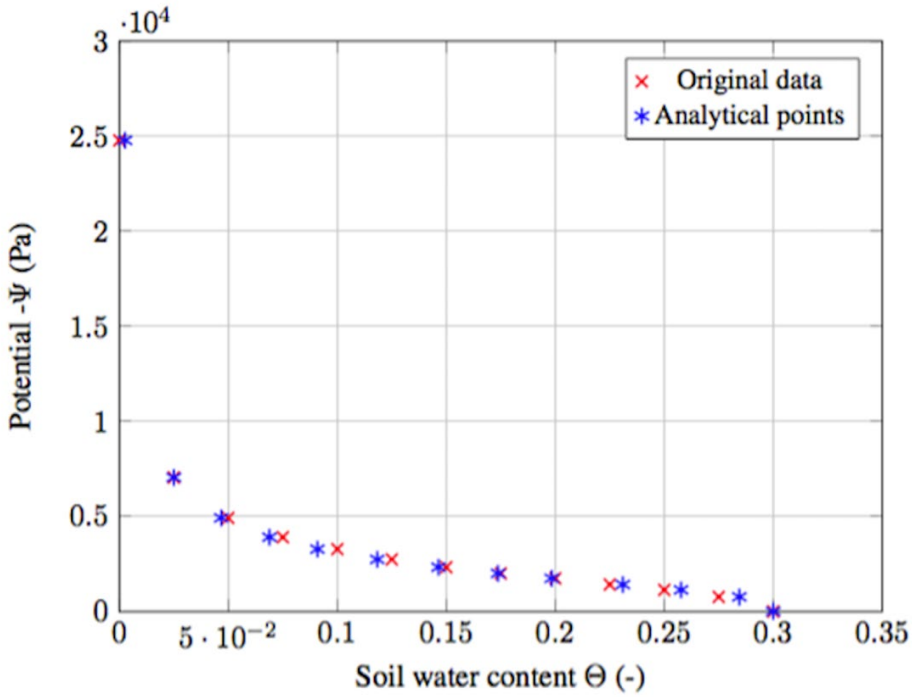

Figure 4: Water Retention Curve (generic) used in the simulations

5. Results

The influencing factors of the simulations are:

- The hydraulic conductivity of the soil where the pipe drain is located equal to 0.00377 m/s, 0.0005m/s and 0.0001m/s
- The soil heterogeneity which can be represented by the ratio between the hydraulic conductivity of the two types of soil, sand and base material, equal to 10, 5 and 2.

This means a total of 9 different scenarios resumed in the following table.

Table 4: Presentation of the 9 different scenarios

Scenario	$K[m/s]$	$\frac{K_1}{K_2}$
Scenario A	3.37710^{-3}	10
Scenario B	3.37710^{-3}	5
Scenario C	3.37710^{-3}	2
Scenario D	110^{-4}	10
Scenario E	110^{-4}	5
Scenario F	110^{-4}	2
Scenario G	510^{-4}	10
Scenario H	510^{-4}	5
Scenario I	510^{-4}	2

For each scenarios a total of 3 different head conditions is considered, as reported in the following.

The different heads represent potential head of the Canal Morto playing as 'reservoir' of the model and taking into account the head losses.

Each scenario allows to estimate a linear regression (the dominant law is the Darcy's Law which is linear) which relates the head and the discharge for linear unit (m^3/sm) as the following example

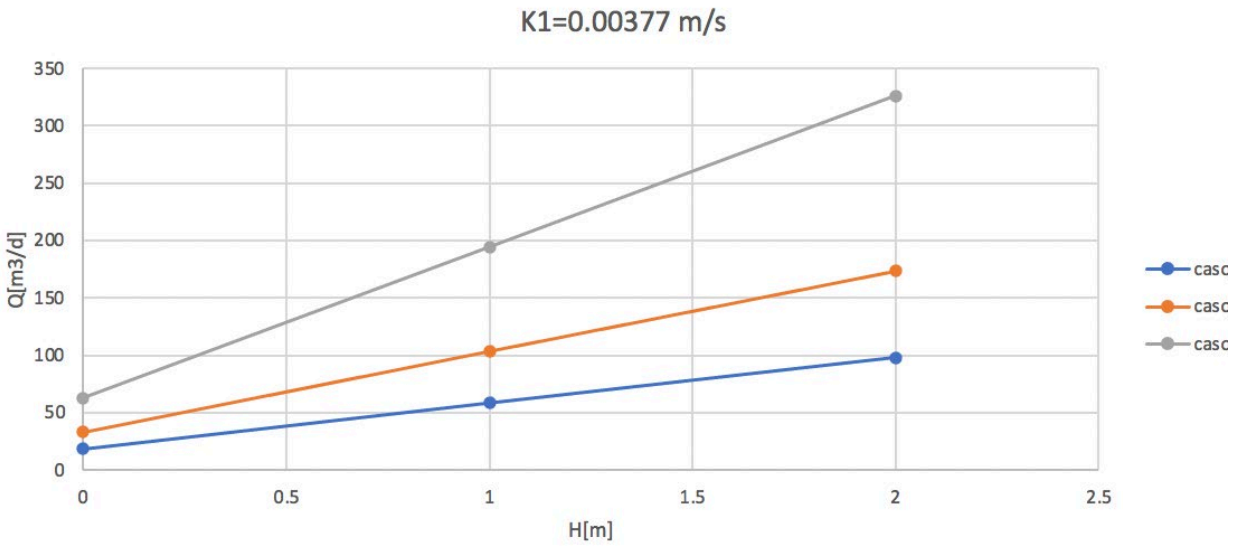

Figure 5: Example of a linear pipe drain relationship for given stratigraphy and and hetereogeneity ratio

where case A refers to a ratio equal to 10, base B equal to 5 and finally case c equal to 2. The 3 different head value are equal to 0 m, 1 m and 2 m starting calculated from the top of the soil.

Each point in the plot represents a single Feflow simulation for given conditions. The aim of the simulations is to estimate at the equilibrium the discharge of the pipe drain, which means the quantity of fresh water provided to the domain by the pipe drainage system. Different heads and different stratigraphy properties are considered.

A synthetic plot of all the scenarios is reported in the log-scale for both the head and the discharge here reported in [l/sm] and [Q/sm].

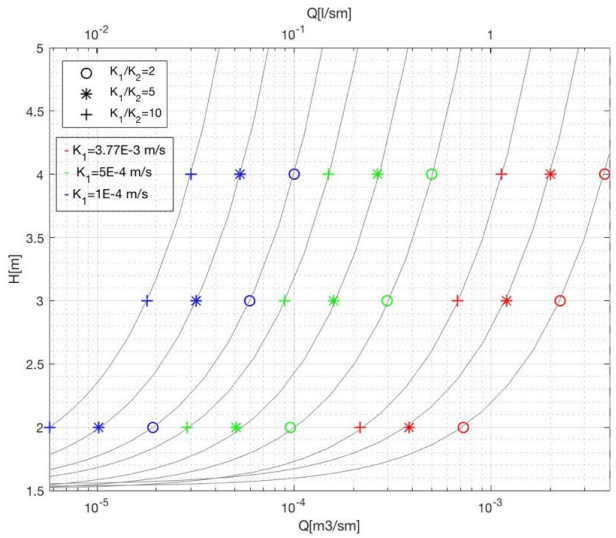

Figure 6: Final log - log plot for different stratigraphy and heterogeneity ratio

Different symbols refer to different level of heterogeneity while the three colors stand for the three different values of hydraulic conductivity of the sand. This plot can be potentially useful to estimate the value of hydraulic conductivity and heterogeneity of the soil when given the head and the discharge flowing from the pipe drain to the domain; on the other hand, in case the head and the stratigraphy of the domain is provided an estimate of the discharge infiltration into the soil to contrast the saltwater intrusion can be obtained (which can be useful for instance to numerically model the pipe drain).

6. Conclusions

The Canal Morto is supposed to supply fresh water to the soil in order to contrast the saltwater intrusion. A drain is installed into the soil to facilitate the distribution of the fresh water of the Canal Morto to the area and prevent saltwater contamination of the crops. The relationship between the Canal Morto water levels and the freshwater discharge needs to be analyzed to verify the pipe drain as potential countermeasure for the seawater intrusion. A conceptual and a numerical model have been developed to estimate the relationship for different stratigraphy and heterogeneity levels. Numerical simulations have been performed in Feflow where the Richards' equations can be applied in a 2D model in transient conditions. These simulations allow to define the relationships between hydraulic heads and the discharge which can be provided by the pipe drain to the domain. The results can be useful to estimate the heterogeneity ratio and the hydraulic conductivity of the soils given the heads and the discharges; on the other hand, when the hydraulic conductivities are known as well as the acting head, the discharge provided by the pipe drain can be estimate, which is crucial for the numerical modeling of the seawater countermeasure.

Section 2

The Italian site 2/2: the site scale

TABLE OF CONTENTS

1. Introduction

Starting from the study conducted in the previous reporting periods, the following analyses are aimed at presenting the insights and new developments of the numerical flow modeling and the preliminary analuiysis of the seawater intrusion samples. Both the diffculties and the seiuccessful results led to conclusion which guide the further developments of the project.

2. Case Study: Mitigation strategies to reduce saltwater intrusion in coastal aquifers: the testing site of Ca' Pasqua, Italy

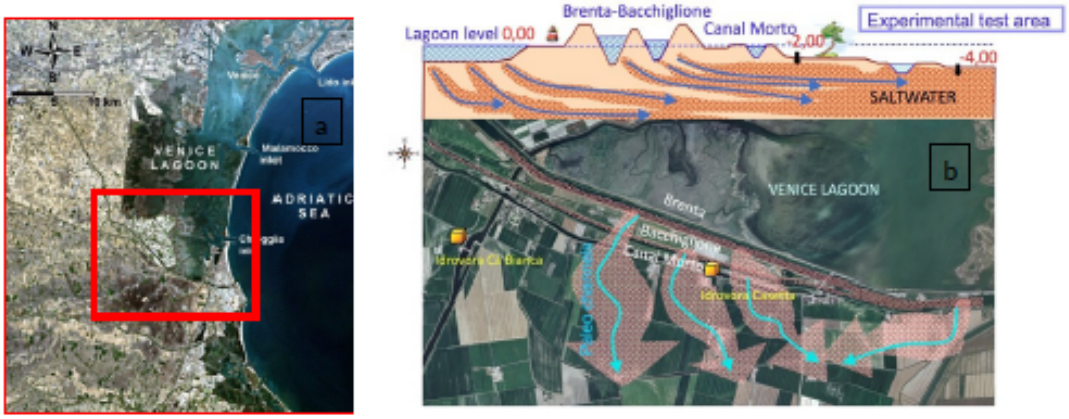

Figure 1: a) General view of the case study in the southern part of the Venetian lagoon. b) Plan view and typical cross-section of the study area, located next to the Casetta pumping station, indicating the main drivers and dynamics of the seawater intrusion.

The study area is complex due to the interplay of different physical elements (e.g. Carbognin and Tosi, 2003): the Bacchiglione and Brenta rivers cross the study area just before flowing into the Adriatic Sea; the Morto channel, whose water level is controlled by a lock gate system, collecting reclamation waters by an upstream pumping station, flows inside the study area, parallel to the Bacchiglione river, while the Venice lagoon lies in the north-east boundary of the domain and in the south-west side there are mainly agricultural fields (Figure 1, panel a) and b)). Seawater intrusion in this reclamation area is dominated by the different elements mainly due to the water levels of the aquifer being lower than the water level in the lagoon, generating a reverse hydraulic gradient. Moreover, the ground surface is below the mean sea level due to land subsidence and the water level in the aquifer is controlled trough a complex system of drains, ditches, and dewatering pumps, to prevent flooding and to control agricultural irrigation. In addition, during dry

periods, the Bacchiglione and Brenta rivers are affected by saltwater intruding from their mouths and traveling upstream. This causes saltwater to intrude in the domain through seepage fluxes from the rivers to the reclamation area. Lastly, a number of paleo-channels have been detected in the area with higher values of hydraulic conductivity which could constitute preferential pathways to the processes.

3. Data availability

Forcings data: updated Casetta and Trezze data

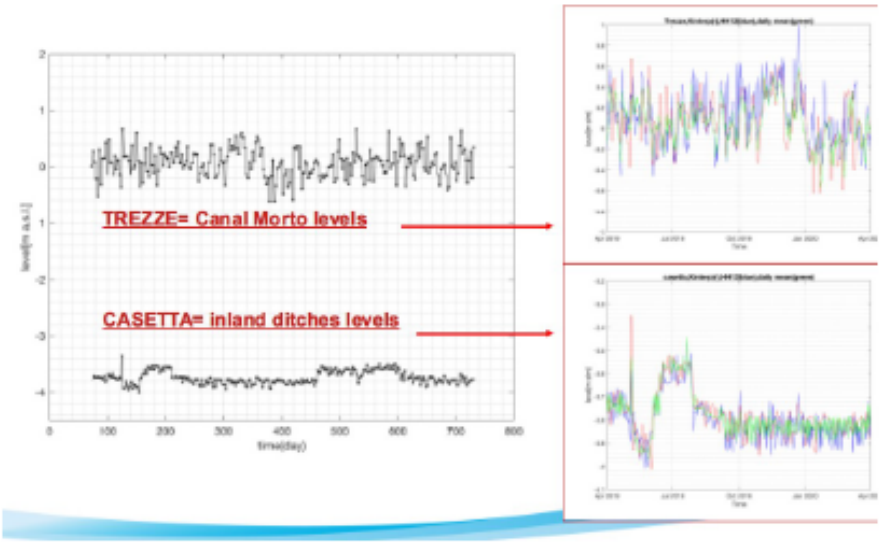

Figure 2: Figure: new Casetta and Trezze data

New Casetta and Trezze data (Figure 2) at a higher time resolution have been kindly providede by the Consorzio di Bonifica Adige euganeo, to more deeply investigated the influence of the complex remediation – irrigation equilibrium characterizing the study area. These data have been applied to each of the following simulations.

4. Modeling activity

The modeling activity required focused on the flow modlling and the transport model.

Model building

Topography analysis and bathymetry estimation

No further modifications on the topography and bathymetry data have been performed

Stratigraphy analysis and soil characterization

The model consists of eight different geological soils which have been estimated starting from field soil-samples, analyzed at the laboratory scale.

- Silt;
- Medium sand
- Silty clay
- Clay – impermeable layer representing the Caranto geological unit
- Sand for the paleochannels in the in-land area and in the whole domain.
- Levees
- Canal Morto cross section
- Brenta and Bacchiglione cross section
- Sand at the surface

Grid definition: layers geometry, resolution

No modification on the grid definition

New preliminary Initial conditions simulations have been performed to estimate reliable initial conditions for the transient state simulations, both for the flow and the saltwater concentration. The initial conditions for the flow simulations are thise obtained at the end of the 6-years transport simulation (futher details in the corresponding sections).Flow simulations

4.1 Stratigraphy and paleo-channel definition

A closer analysis of the provided stratigraphy has been performed which shows the presence of a big lense of sand on the top surface. The analysis highlighted the importance of create a 'new' sand material for the surface.

4.2 Boundary condition estimation and definition

Each day is applied at a daily resolution. Close attention has been paid the analysis and application of the boundary conditions in the in-land part of the domain which play the major role to protect the maize crops. The latest Trezze levels have been scaled at a daily resolution and applied to the Canal Morto for which at the beginning constant levels data has been considered. Finally, Casetta levels are essential to the definition of the dynamics of the main ditches (2) and consequently the draining network in the in-land part of the domain where the irrigation to the crops is to be guaranteed by the Land Reclamation Consortium. New potential boundary conditions have been tested together with the applicatuion of a further package in the model which takes into consideration the vadose zone dynamics. This aspect, together with the definition of the evapotranspiration and consequantly the net rain allowed to defined the recharge as explained in the following section.

4.3 Recharge estimation

The recharge spatial and temporal distribution has been estimated by applying the rain and net rain together with the vadose zone module at the However, results seems not to be able to fully reproduce the effect of the real recharge. This aspect will be further analyhsed in gthe following period.

4.4 Hydraulic parameters optimization – manual calibration

Authomatic parameters estimation have been attempted n the SEAWAT envoronment. A number oftest have been carried out with different number of parameters and different existence ranges.

Salt water intrusion

The saltwater intrusion simulations have been performed at a preliminary scale (monthly resolution and constant level for the Canal Morto); the salt concentration ranges from 0 kg/m³ to 35 kg/m³. The lagoon area is supposed to provide saltwater at the highest constant concentration. The Brenta and Bacchiglione rivers provide saltwater to the domain because of the intruding from their mouths and traveling upstream, causing saltwater to intrude in the domain through seepage fluxes at a variable concentration. Canal Morto is supposed to provide only fresh water. A 6-years simulation has been carried out to define the flow and transport initial conditions of the main simulations.

5. Results and discussion

General considerations

The simulations highlight a high vulnerability level of the area to the saline intrusion phenomenon due to the inner hydrological and geomorphological features of the site; a number of acting forgings play a role in the global dynamics of the phenomenon, which need to be carefully estimated and globally weighted in order to define how and how much the different acting forcings influence the phenomenon in reality, and consequently the simulations; indeed, the dynamics of the phenomenon poses a quite high complexity problem; furthermore, each elements of the model - starting from the topography to the definition of the type of boundary conditions to the location of the paleo-channels, to mention but a few – introduce a level of uncertainty to the modeling activity which has to be considered and quantified: this is why a sensitivity analysis on the major influencing factors is needed, especially regarding the major parameters such as the hydraulic conductivity of the different soil - manually or automatically - to provide reliable scenarios and to properly design the most performing mitigation strategies. More in detailed the numerical modelling of the vadose zone seems to play a major role in the overwhole flow and transport dynamics as the location of the water tables and consequently of the fluxes is quite superficial.

Model building results

The simulation highlighted the importance of a more complex stratigraphycal model which taken into consideration also a different conductivity of the levees and the brenta ane bacchiglione riverbeds.

Flow results

A number of flow scenarios have been performed in order to properly define two main aspects.

i)Proper definition of the boundary conditions, ii) application of the vadose zone, iIi) a proper estimation of the main influencing parameters and and finally iv) authomatic parameter estimation with PEST.

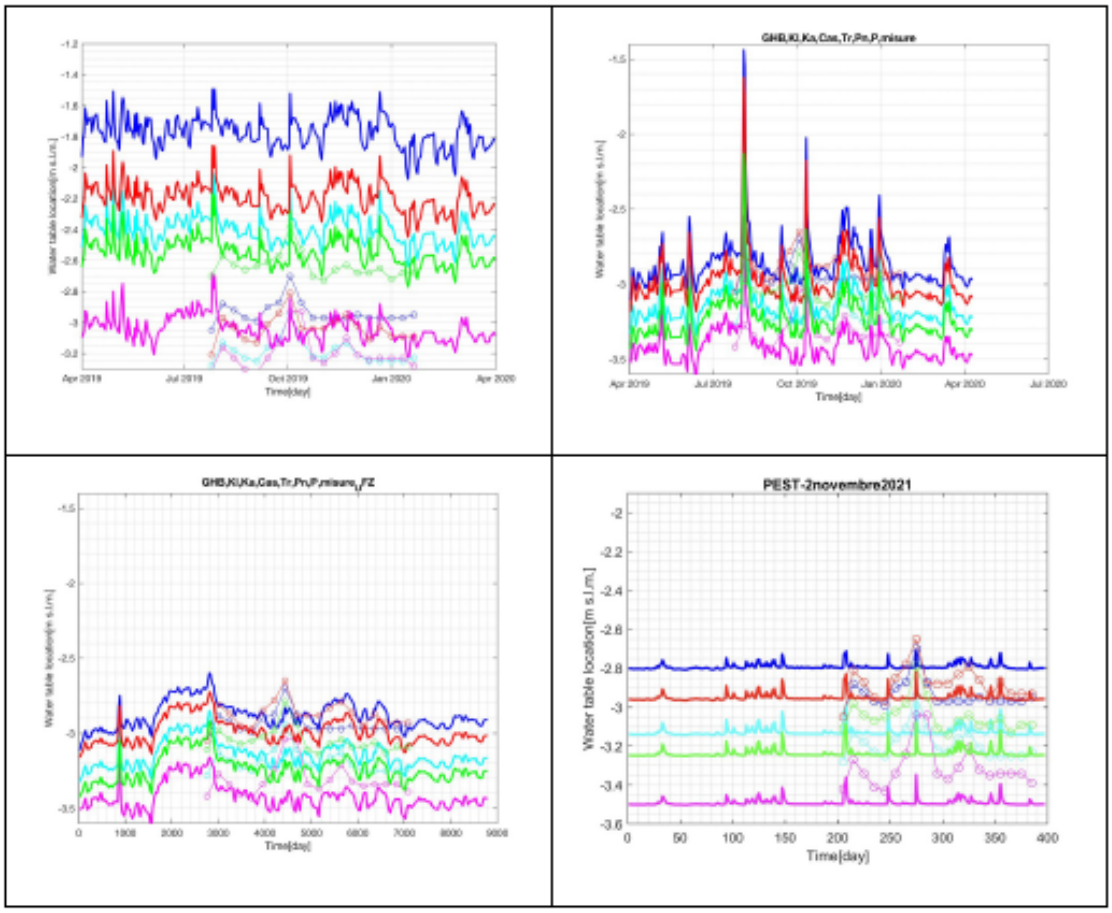

Figure 3 : simulated results for the 5 measurements station located at Ca' Pasqua (solid line) compared to the measures (thin lines) for the simulation year ij four major cases: from the top left: the results reported in report period V, top-right the application of the GHB boundary conditions for the dicthes network,

bottom-left the application of the UZF package for the vadose zone and finally the application of the DRAIN conditions for the ditches network.

GHB boundary conditions for the inland ditches network have been applied tested providing performing results with and without considering the vadose zone. However, problem in the final part of the inland model suggesting to shift to the drain conditions as reported in figure (3). This solitions however does not help in reproducing properly the dinamics of the water tables while obtaining a good match in tems of mean water table position. The PEST simulations have been performed in this last case, with the drain options active. A number of diffeent attempts has been tested, using different existence ranges and with different sets of parameters (figure 4).

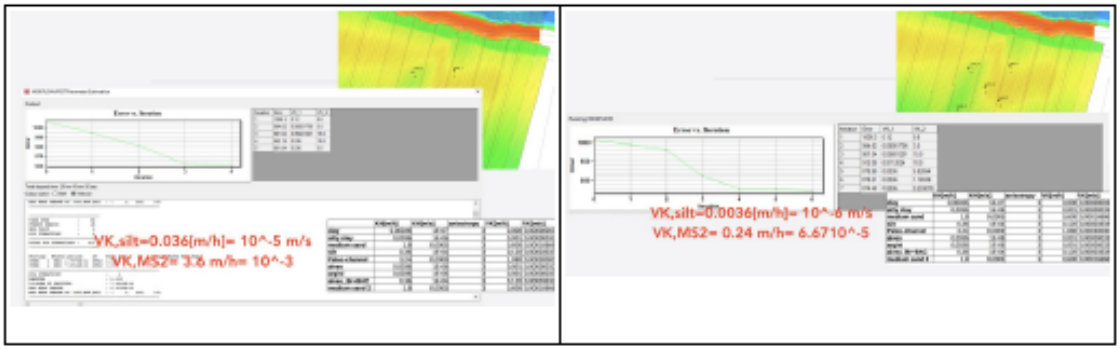

Figure 4: two samples of PEST procedure using different existence ranges and parameters.

Difficulties in reproducing the prope dynamics and in converging with the PEST simulations led to the idea that of futher investigated the physical dynamics of the flows: this ed to the conclusion that the exchange processes between the water table and the ditches network need to be further analyzed and the infiltration mechanism of the net rain plays a role, as it can be seen in figure 5 where two different precipitation apporoaches have been compared and where the the water table measurements and the net rain dynamics are quite syncronized. Given these results a more detailed analysis of the infiltration process and the exchange of water between the ditches and the watertable is necessary using a software where the whole dynamics is treated with Richards' equations.

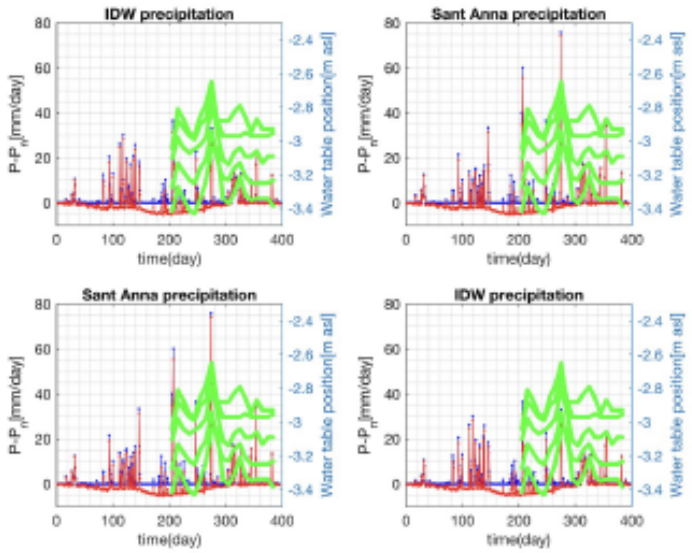

Figure 5: Rapresentation of the precipitation (blue), net precipitation (red) and water table locations (green) in time.

Transport results

Preliminary transport results took into consideration both the advective and the dispersion and diffusion processes, where the dispersion action appears more signifocant as previously though. A 6-years transport model has been set up gto obtain reliable initial flow and above all transport conditions.

In general, as already seen during the previous reporting period, it can be appreciated that no infiltration is reported in the caranto – clay layer which can be considered impermeable; if we look at the dynamics along a longitudinal cross section it can be appreciated that the concentration move from the lagoon to the in-land part, while the concentration coming from the rivers intrude radially and tends to move towards the in-land part of the domain from the bottom to the top: indeed, the salt plume has to move further the Canal Morto which is supposed to provide fresh water; looking at a transversal cross section of the in-land part of the domain can be appreciated the dominant role of the ditches network and the preferential salt water intrusion pathway of the paleo-channels.

In figure 6 the evolution of the instuding front can be appreciated in years in particular, it was necessary to iterate the simulations in order to obtain a reliable salt water field in the final part of the inland domain where the second guard ditch is located to avoid stagnation of the salt water.

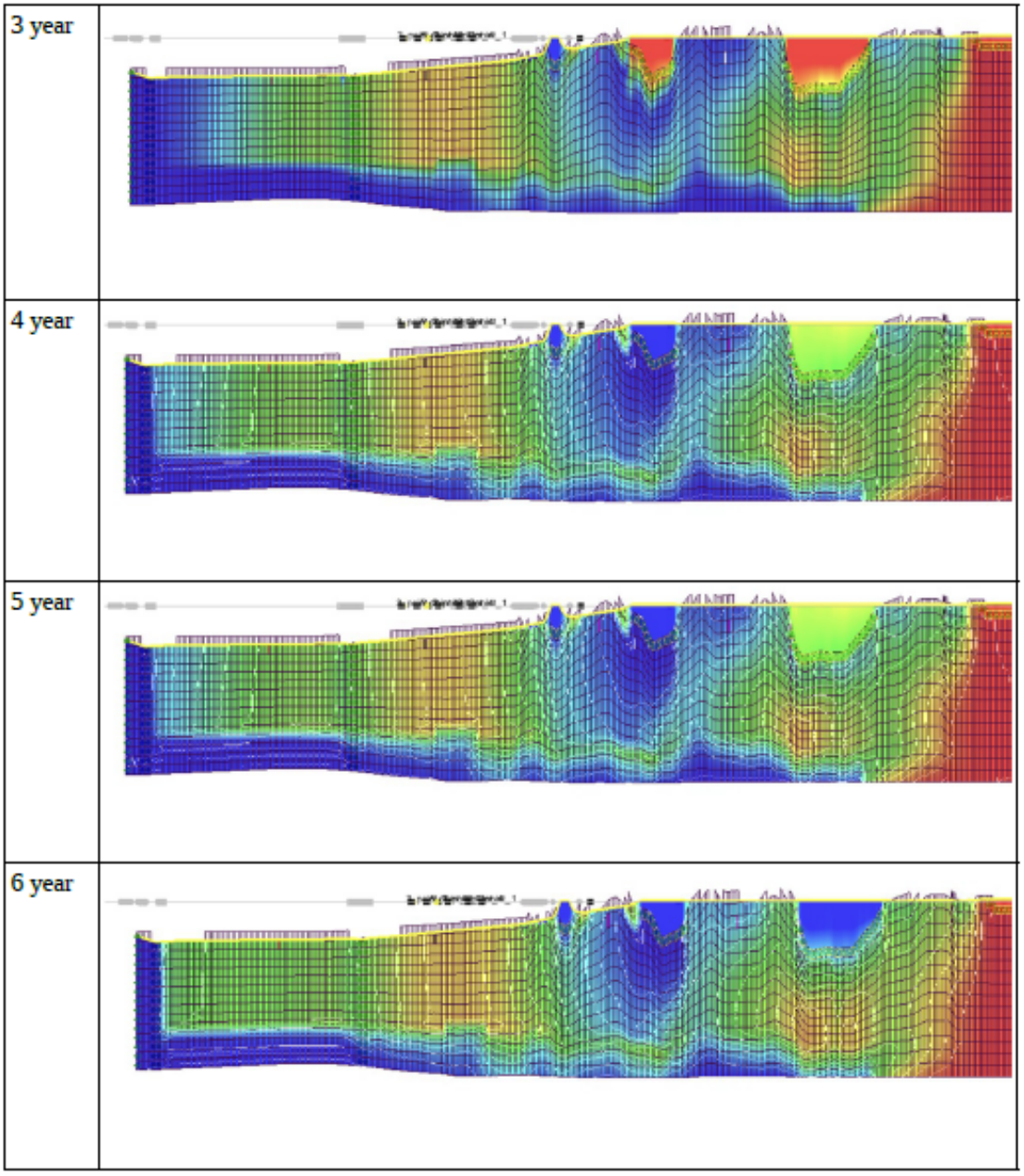

Figure 6: evolution of the salt water intrution for the difinition of the transport initial condotions.

10

Section 3

The Croatian site

Project: “Monitoring Sea-water intrusion in coastal aquifers and Testing pilot projects for its mitigation” Interreg CBC Italy-Croatia 2014.-2020.

Priority Axis: Safety and resilience

Specific objective: Improve the climate change monitoring and planning of adaptation measures tackling specific effects, in the cooperation area

(D_3.4.5) Report on the model application to evaluate the efficiency of mitigation strategies for the selected scenarios of climate changes

Work Package 3: Studying

Activity 4: Numerical modelling

Partner in charge: PP4 (UNIST-FGAG)

Partners involved: PP4 (UNIST-FGAG), PP5 (CROATIAN WATERS), PP6 (DUNEA)

Final version

Public report

September, 2022

Contents

Aims and scopes

As a part of MoST project, numerical model that describes existing state of head distribution and salinity regime in the area of River Neretva Valley was made. The model was calibrated and verified on measured time series of piezometric head and concentration values on seven piezometers located in the valley.

This report is made to define scenarios of climate changes that predominantly effect the area of River Neretva Valley and offer suitable mitigation measures suitable to be done on Croatian project site as an activity proposed by the project: “Monitoring Sea-water intrusion in coastal aquifers and Testing pilot projects for its mitigation” Interreg CBC Italy-Croatia 2014.-2020.

Presented climate change scenarios will be based on models made for relevant global, European and Croatian agencies. Numerical modelling will be done for selected scenarios.

Based on the effects done by climate changes, mitigation measures will be presented. Presented mitigation measures will be made based on specificities of River Neretva Valley and will incorporated in existing system.

In continuation all climate change and mitigation measures scenarios are explained and model results are shown.

Scenarios of climate changes

Change in temperature

Based on projected changes in ground air temperature, precipitation and mean sea level shown for global, European and Croatian area it is possible to conclude that changes are inevitable but values of changes vary based on projected scenarios (SSP2 – SSP5).

Based on EEA, ground air temperatures in Europe are projected to increase by 1.2 to 3.4° under the SSP1-2.6 scenario and by 4.1 to 8.5°C under the SSP5-8.5 scenario (by 2071-2100, compared to 1981–2010).

Based on DHMZ ground air temperatures in Croatia in the first period (2011-2040), are expected to rise up to 0.6 ° C for winter and up to 1 ° C for summer period. In the second period (2041-2070), the expected growth of the ground air temperature in Croatia is up to 2 ° C in the continental part and up to 1.6 ° C in the south for the winter period, and up to 2.4 ° C in the continental part of Croatia, and up to 3 ° C in the coastal zone for the summer period.

CCKP data show monthly mean temperature changes increasing by 1.36°C by the 2030s to more than 4°C by the 2090s.

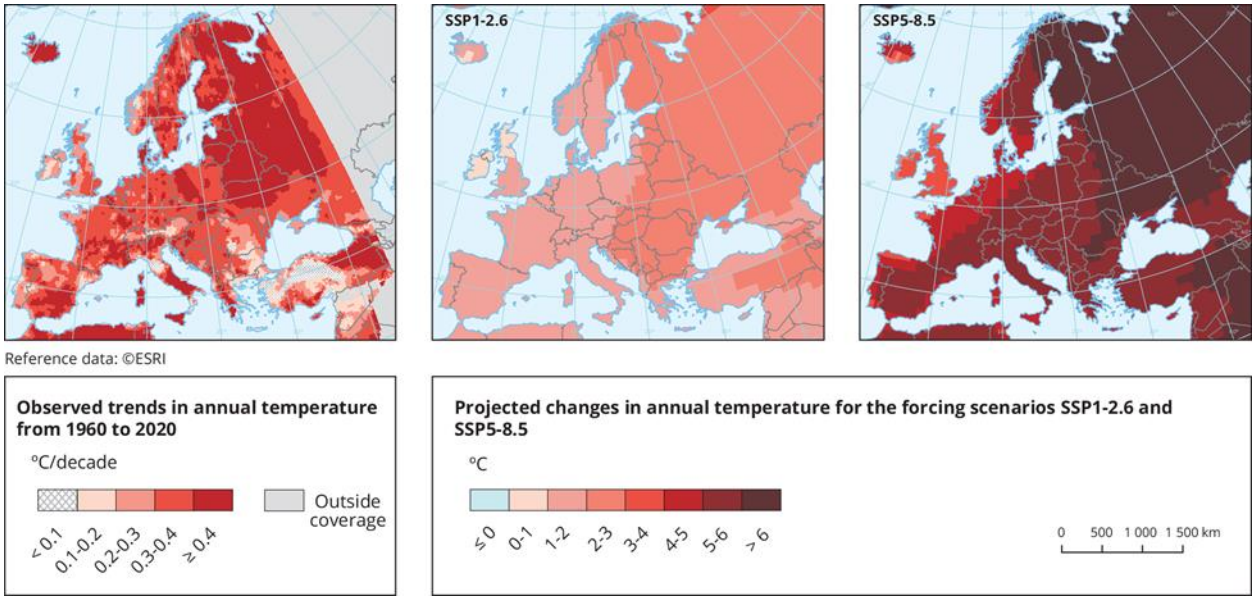

Figure 1 Observed annual mean temperature trend from 1960 to 2020 (left panel) and projected 21st century temperature change under different SSP scenarios (right panels) in Europe [5]

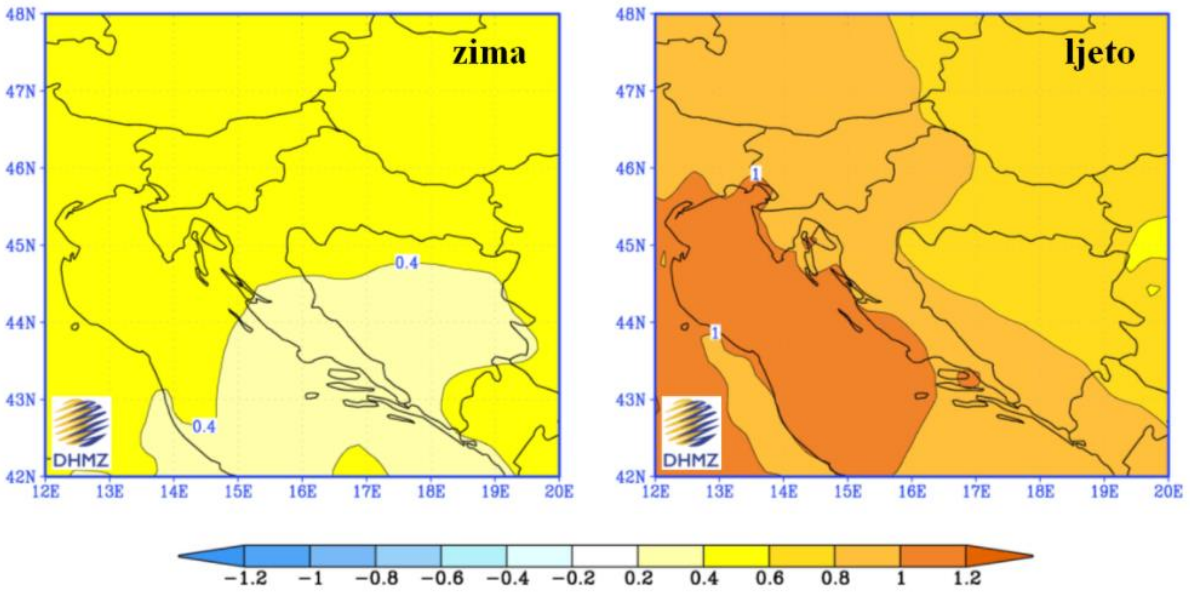

Figure 2 Change in ground air temperature (in ° C) in Croatia in the period 2011-2040 compared to the period 1961-1990 according to the results of the middle class of the RegCM regional climate model ensemble for A2 greenhouse gas emission scenario for winter (left) and summer (right)). (https://meteo.hr/klima.php?section=klima_modeli&param=klima_promjene)

Change in precipitation

EEA models project an increase in annual precipitation in large parts of central and northern Europe (of up to about 30 %) and a decrease in southern Europe (of up to 40 %) from 1971–2000 to 2071–2100. In summer, the precipitation decrease extends northwards. Values of projected change in annual precipitation for Croatian area based on Figure 10 is -5 to 5% and values od projected change in summer precipitation is -30 to -20%.

Based on DHMZ regional climate model, changes in precipitation in the near future (2011-2040) are very small and vary depending on the season. The largest change in precipitation can be expected in the Adriatic in the autumn with a decrease in precipitation with a maximum of approximately 45-50 mm. In the second period (2041-2070), change in precipitation in mountainous Croatia and in the coastal area will reach a value of 45 - 50 mm.

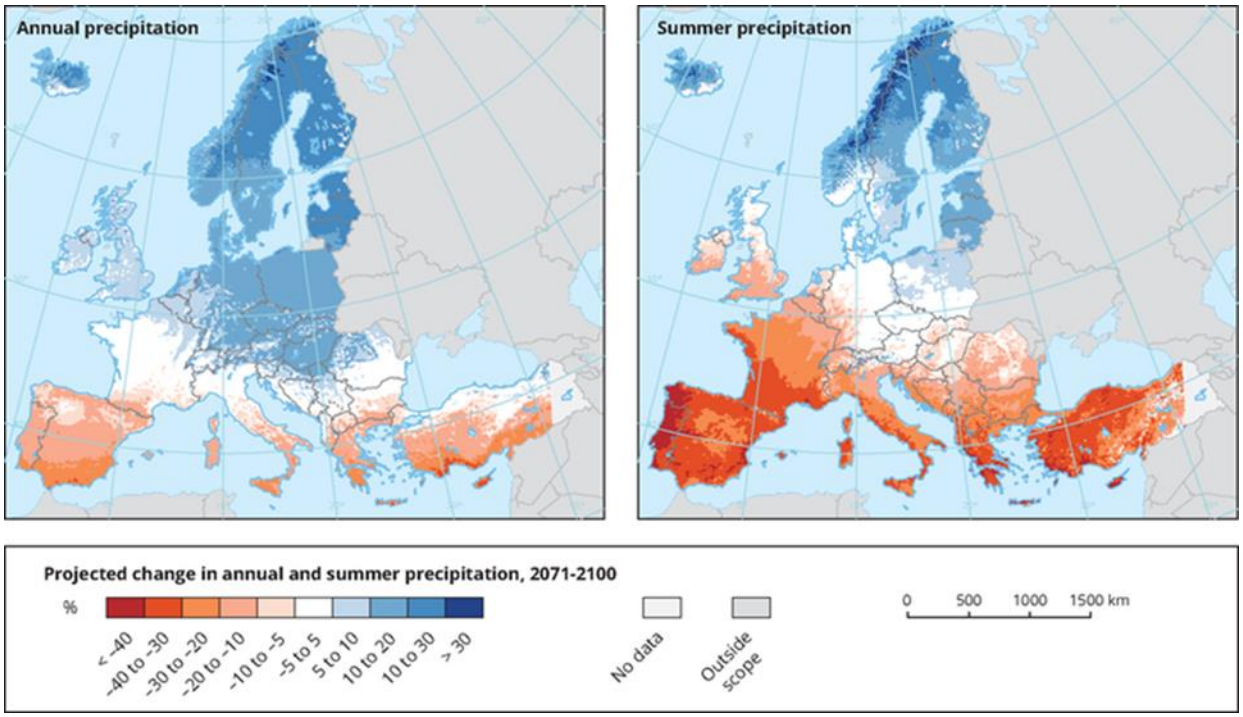

Figure 3 Projected changes in annual (left) and summer (right) precipitation (%) in the period 2071-2100 compared to the baseline period 1971-2000 for the forcing scenario RCP 8.5. Model simulations are based on the multi-model ensemble average of RCM simulations from the EURO-CORDEX initiative. (https://www.eea.europa.eu/data-and-maps/figures/projected-changes-in-annual-and-5)

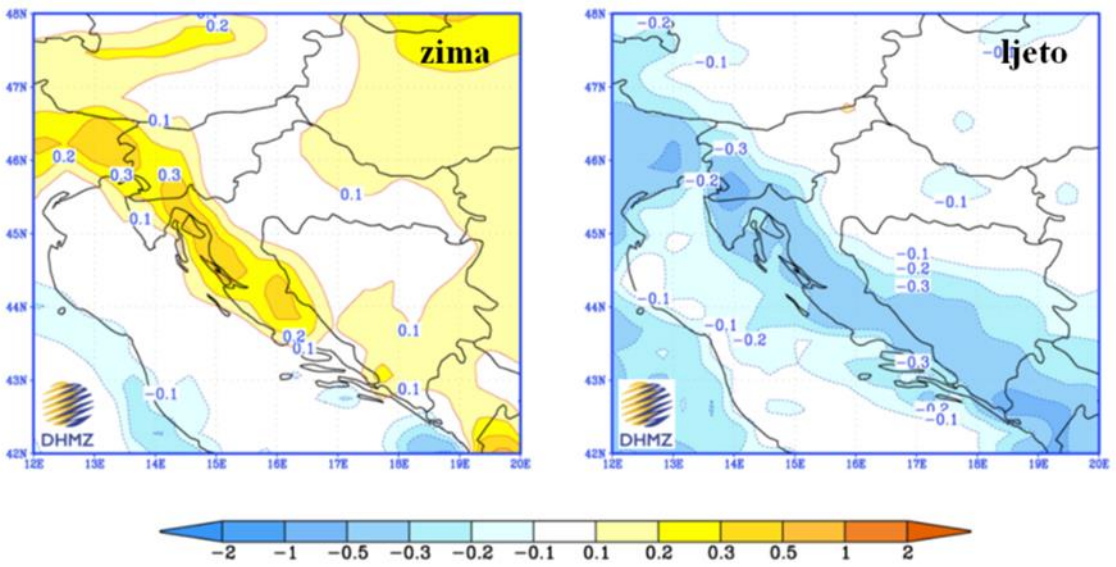

Figure 4 Change in precipitation in Croatia (in mm / day) in the period 2041-2070 compared to the period 1961-1990 according to the results of the middle class of the RegCM regional climate model ensemble for A2 greenhouse gas emission scenario for winter (left) and summer (right). (https://meteo.hr/klima.php?section=klima_modeli&param=klima_promjene)

Change in sea level

Based on EEA, global mean se level will rise by 0.28-0.55 m under a very low emissions scenario (SSP1-1.9) and 0.63-1.02 m under a very high emissions scenario (SSP5-8.5) by 2100, relative to the 1995-2014 average. Based on Figure 16 projected rise in sea level during 21st century in Croatian area will be 0.4 to 0.5 m.

Based on IPCC, global mean sea level will rise between 0.43 m (0.29–0.59 m, RCP2.6) and 0.84 m (0.61–1.10 m, RCP8.5) by 2100 relative to 1986–2005.

Based on [16] mean sea level in central and southern Adriatic will increase around 40 cm over the next hundred years, which is in line with IPCC and EEA forecasts.

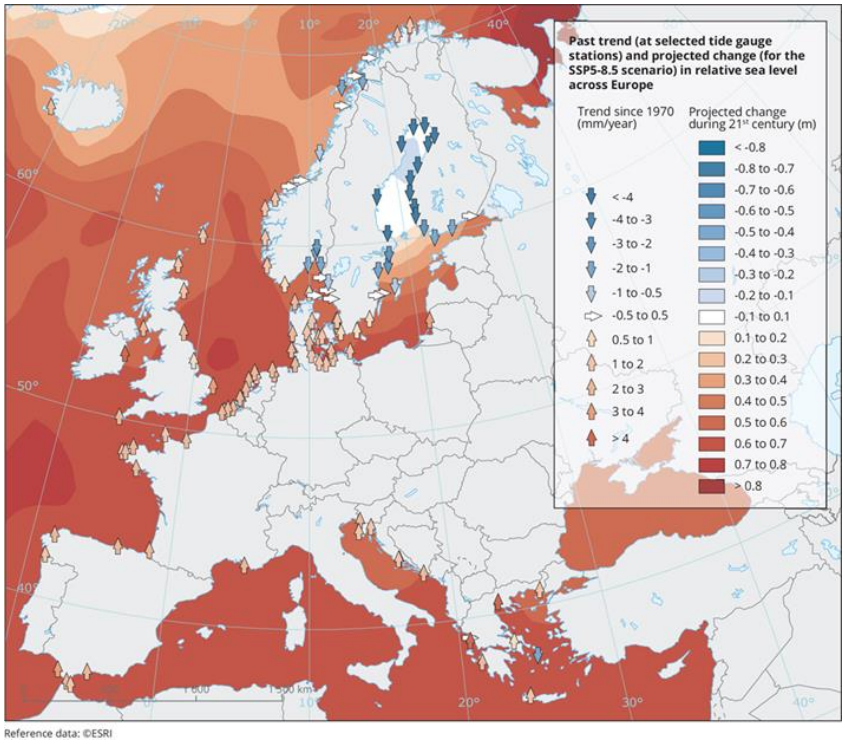

Figure 5 Past trend and projected change in relative sea level across Europe (https://www.eea.europa.eu/ims/global-and-european-sea-level-rise)

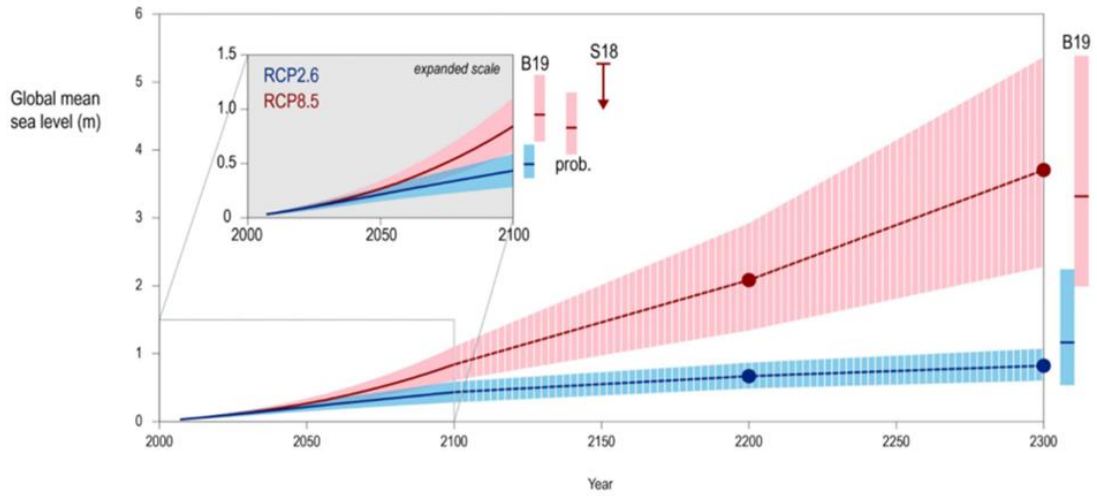

Figure 6 Projected sea level rise (SLR) until 2300 (https://www.ipcc.ch/srocc/chapter/chapter-4-sea-level-rise-and-implications-for-low-lying-islands-coasts-and-communities/)

Selected scenarios of climate changes

Change in sea level

Based on EEA and IPCC predictions for the change of sea level, two scenarios were tested:

- Sea level rise for 43 cm
- Sea level rise for 84 cm

Climate change scenarios in the model were tested in transient constant simulation.

Flow boundary conditions for climate change simulations were mean values of boundary condition determined for existing state simulations. The only change was made on determination of sea boundary condition and its value was determined based on climate change scenario. All values were set as constant transient values for 160 stress periods. Flow initial condition for climate change simulation were head results of flow steady state simulation.

Transport boundary conditions for climate change simulation was concentration value of 36 g/l along the sea line and in River Neretva. Boundary conditions for Opuzen, Mala Neretva and channels were defined as $dC/cX \neq 0$, $dC/dZ \neq 0$. Transport initial condition for climate change simulation were the values of concentration obtained in flow and transport steady state simulation.

Sea water boundary condition was defined with CHD package (The Constant Head Designation) in the model. The values were determined based on climate change scenario and that is increase for 43 or 84 cm based on scenario. Figure 7 shows position of sea boundary condition in the model.

Figure 7 Sea boundary condition defined in the model

Change in precipitation

Based on EEA and DHMZ predictions for change in precipitation, two scenarios were tested:

- 10% precipitation decline
- 20% precipitation decline

Climate change scenarios in the model were tested in transient constant simulation. Transient constant simulations were set for a long period of time (around 100 years) and the usage of RCH Package for precipitation description was not possible. Instead of using RHC Package for precipitation description, flow boundary condition was used and it represented inflow in the model due to precipitation.

Flow boundary conditions for climate change simulations were mean values of boundary condition determined for existing state simulations. The only change was flow boundary condition and its value was determined based on climate change scenario. All values were set as

constant transient values for 160 stress periods. Flow initial condition for climate change simulation were head results of flow steady state simulation.

Transport boundary conditions for climate change simulation was concentration value of 36 g/l along the sea line and in River Neretva. Boundary conditions for Opuzen, Mala Neretva and channels were defined as $dC/cX \neq 0$, $dC/dZ \neq 0$. Transport initial condition for climate change simulation were the values of concentration obtained in flow and transport steady state simulation.

Figure 8 Flow boundary condition

Results of climate change modelling

Model response due to sea level rise

Next figures show changes in salinity field for the layer of sand and the layer of gravel due to sea level rise. Simulations were set on flow and transport steady state simulation obtained for existing state. Simulations were set for 160 years and in that period steady state for head and for concentration is achieved for all locations.

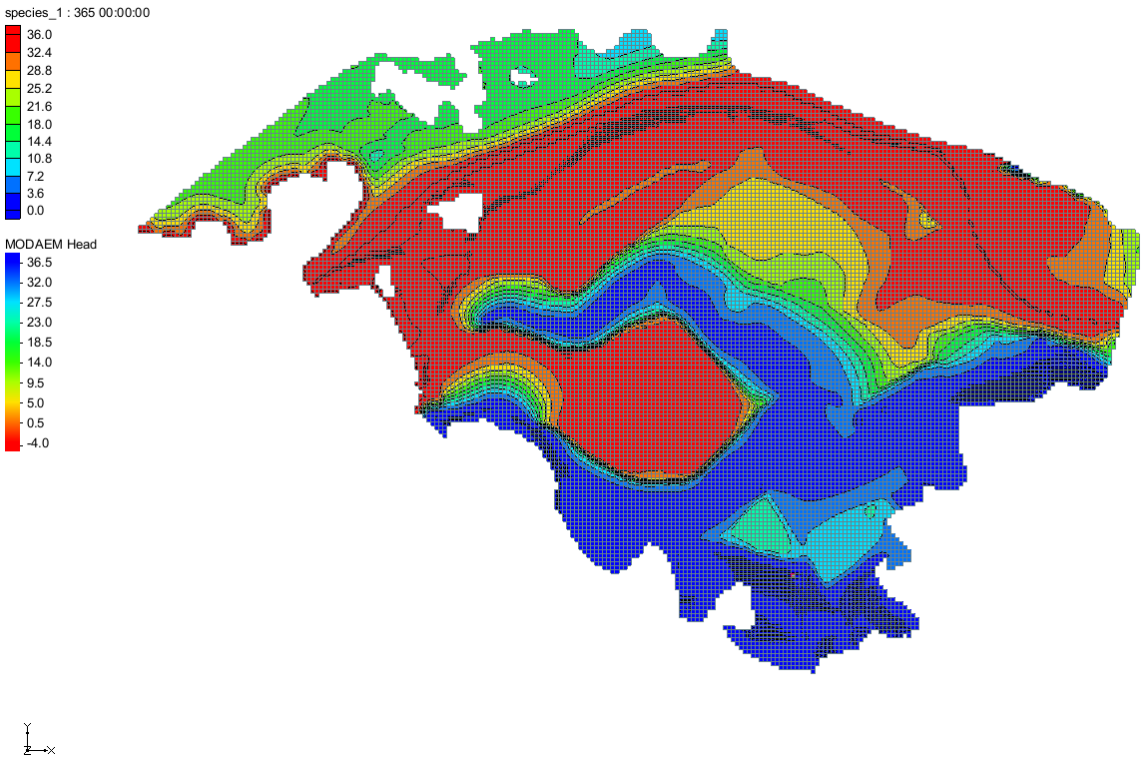

Figure 9 Salinity field for the layer of sand before climate changes

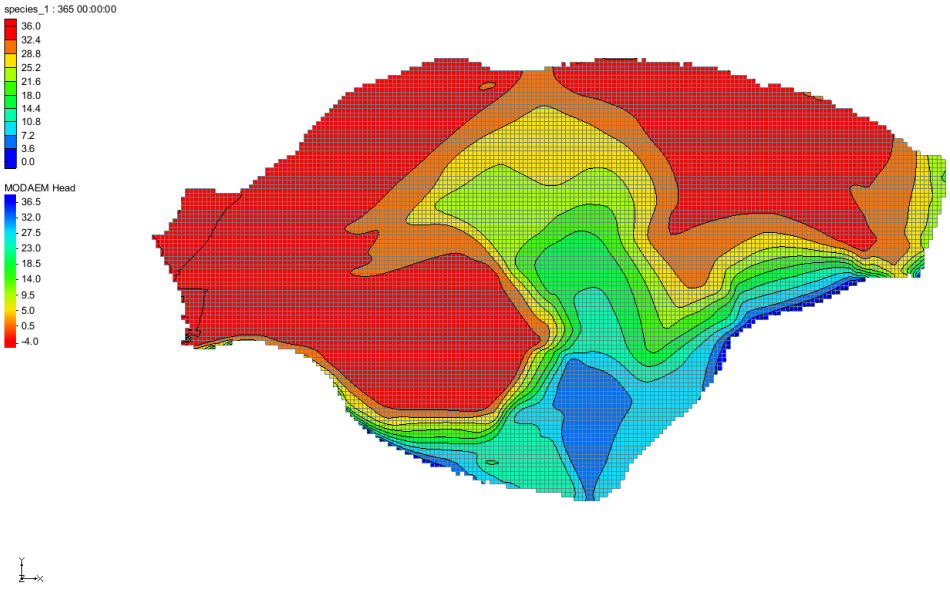

Figure 10 Salinity field for the layer of gravel before climate changes

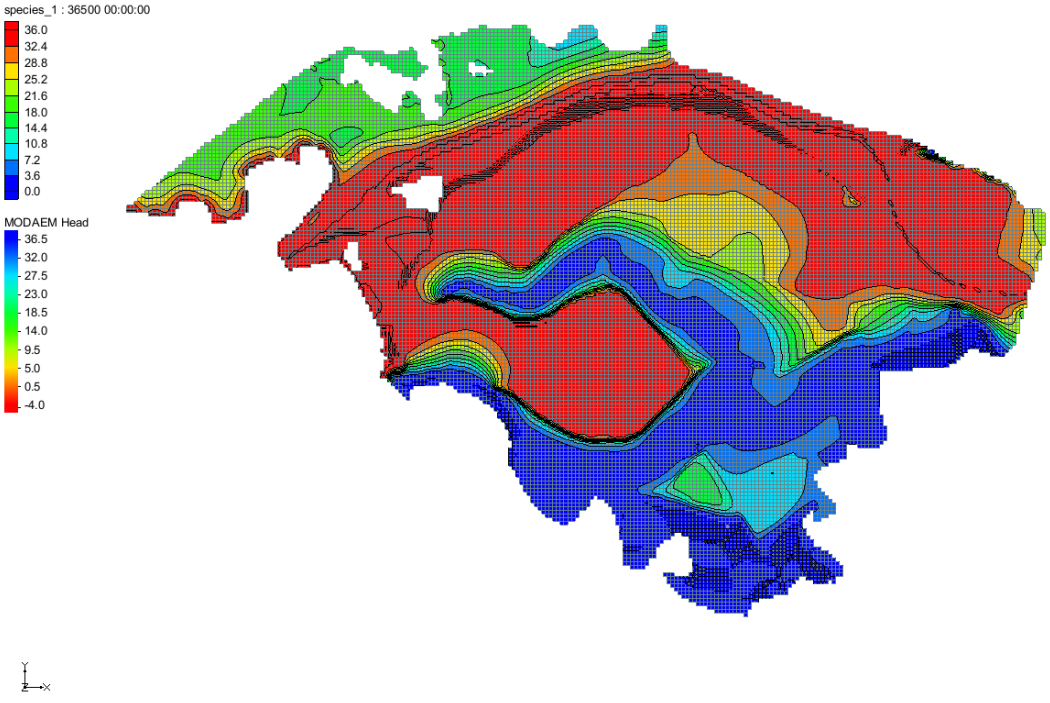

Figure 11 Salinity field for the layer of sand after 160 years of SLR for 43 cm

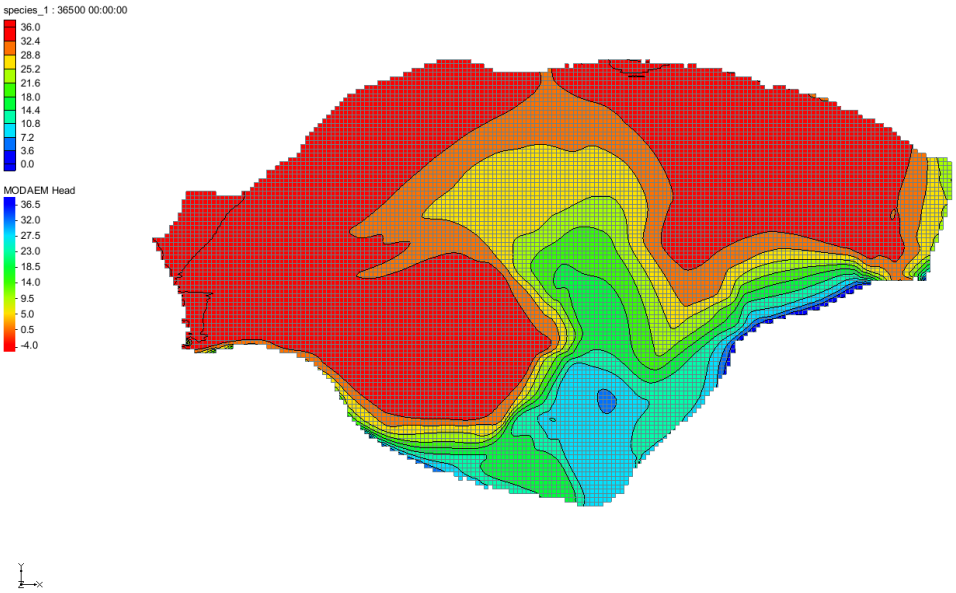

Figure 12 Salinity field for the layer of gravel after 160 years of SLR for 43 cm

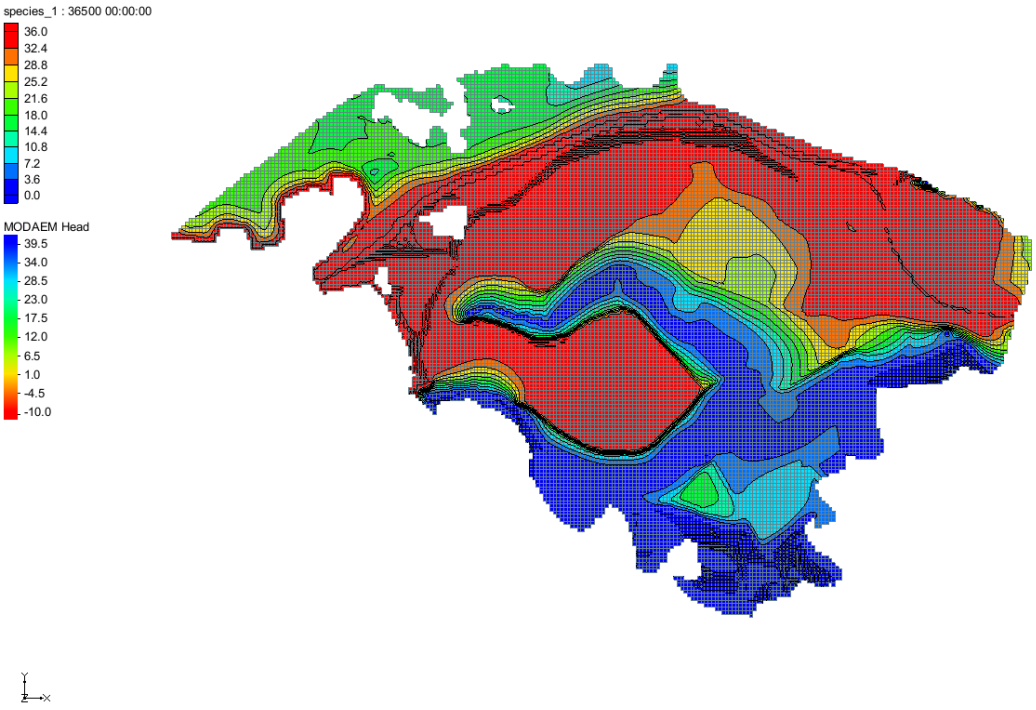

Figure 13 Salinity field for the layer of sand after 160 years of SLR for 84 cm

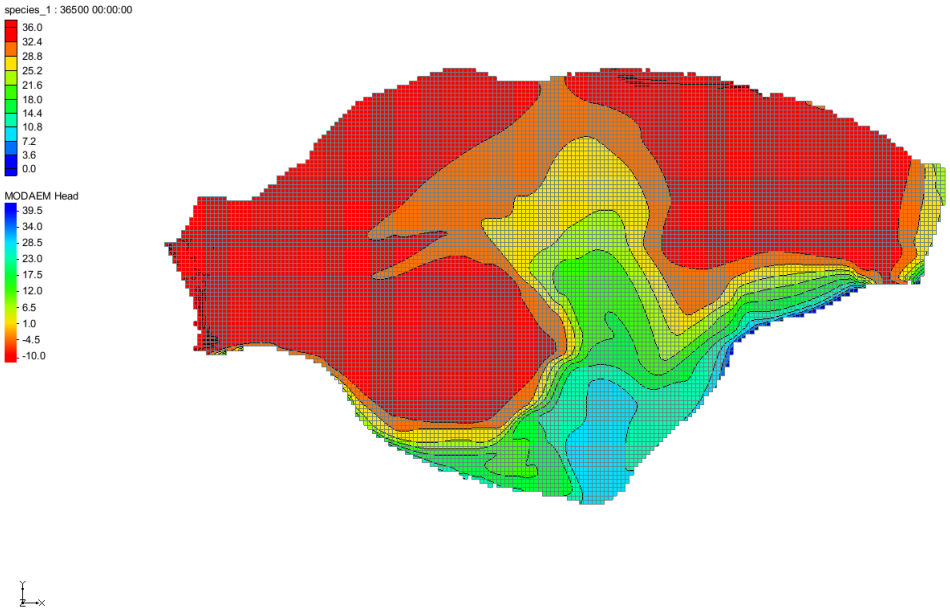

Figure 14 Salinity field for the layer of gravel after 160 years of SLR for 84 cm

Next figures show the change of head and concentration for three shallow piezometers (P1, P2 and P4) and for four deep piezometers (D1, D2, D3 and D4) due to sea level rise.

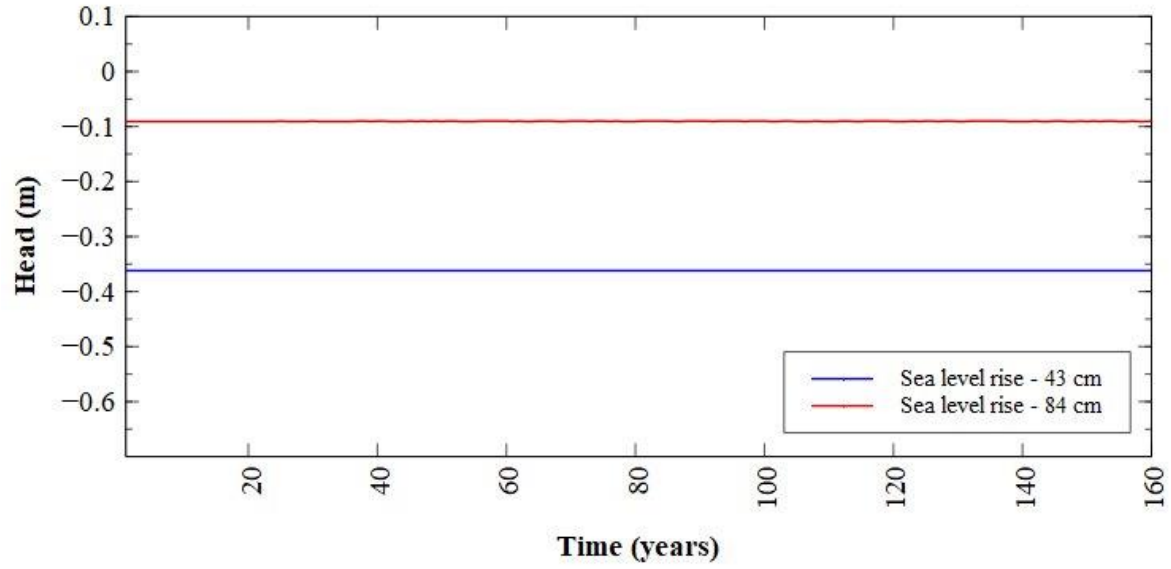

Figure 15 Change of head for piezometer P1 for sea level rise for 43 and 84 cm

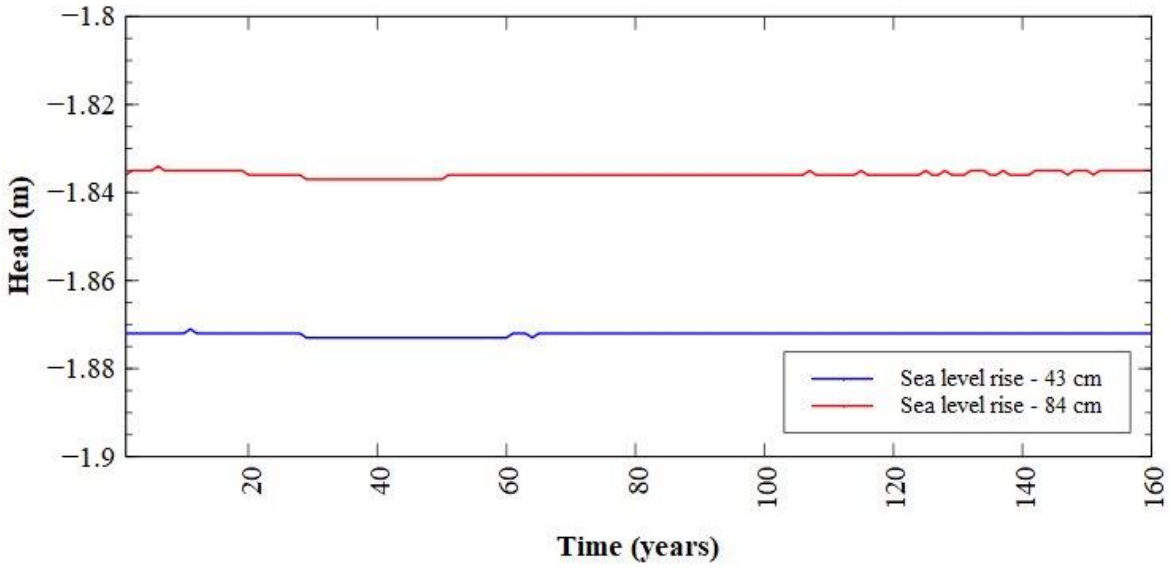

Figure 16 Change of head for piezometer P2 for sea level rise for 43 and 84 cm

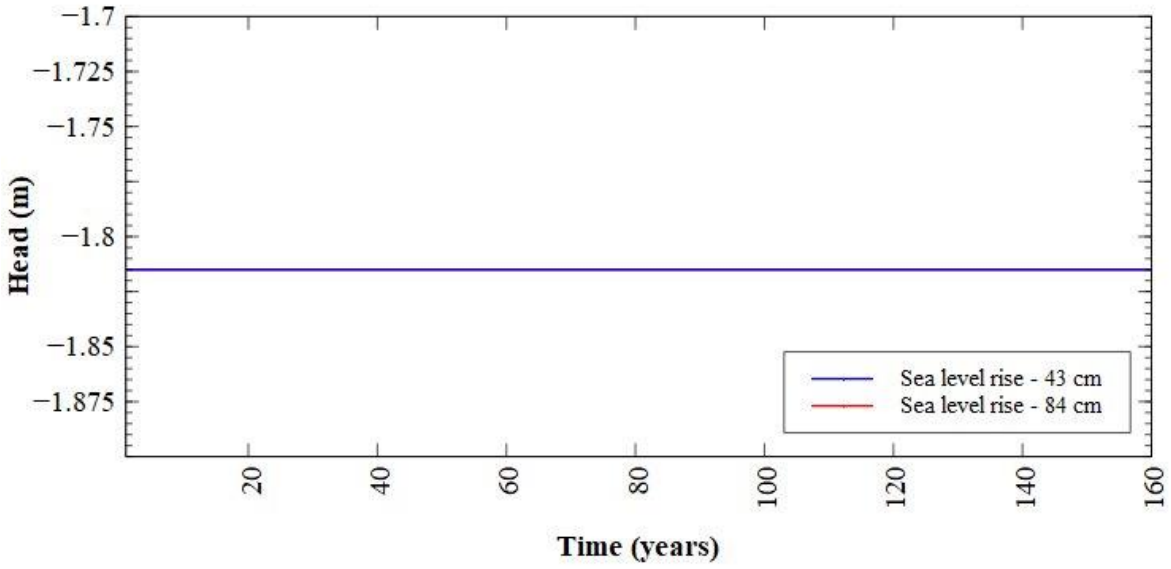

Figure 17 Change of head for piezometer P4 for sea level rise for 43 and 84 cm

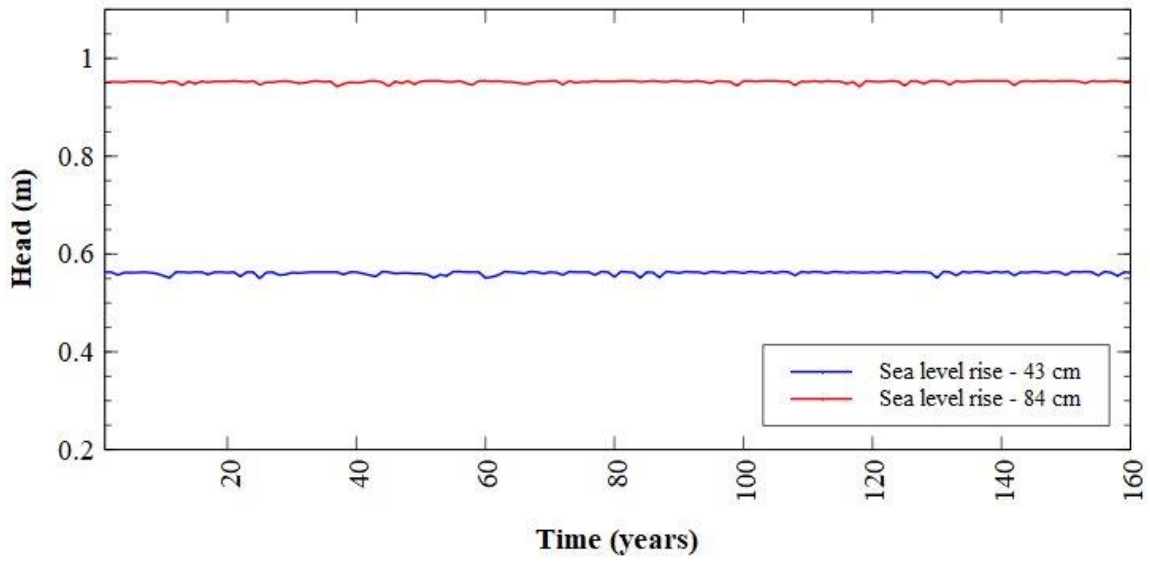

Figure 18 Change of head for piezometer D1 for sea level rise for 43 and 84 cm

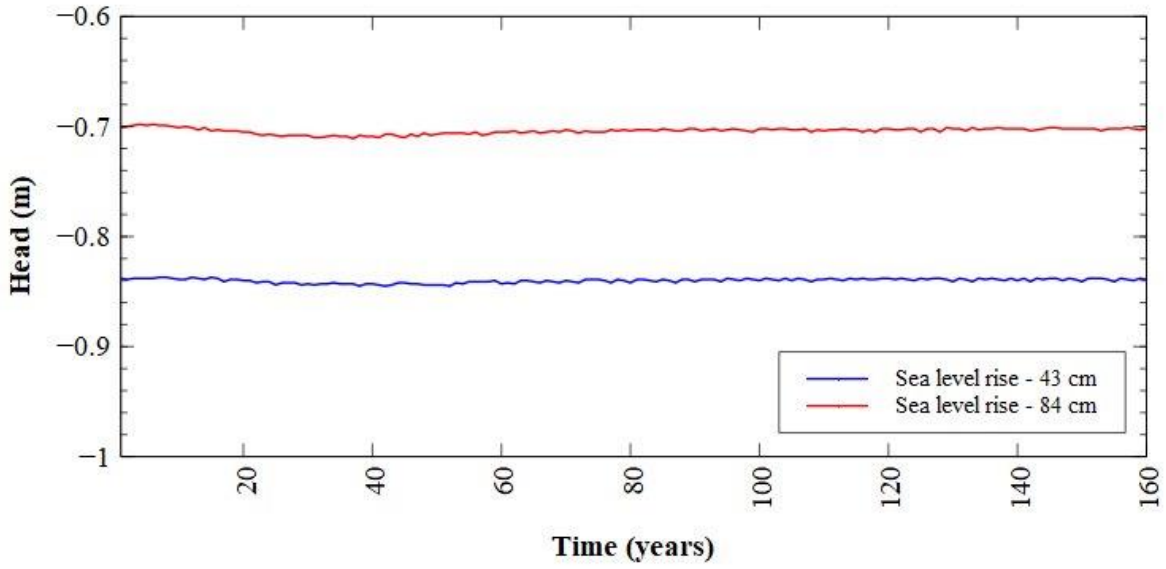

Figure 19 Change of head for piezometer D2 for sea level rise for 43 and 84 cm

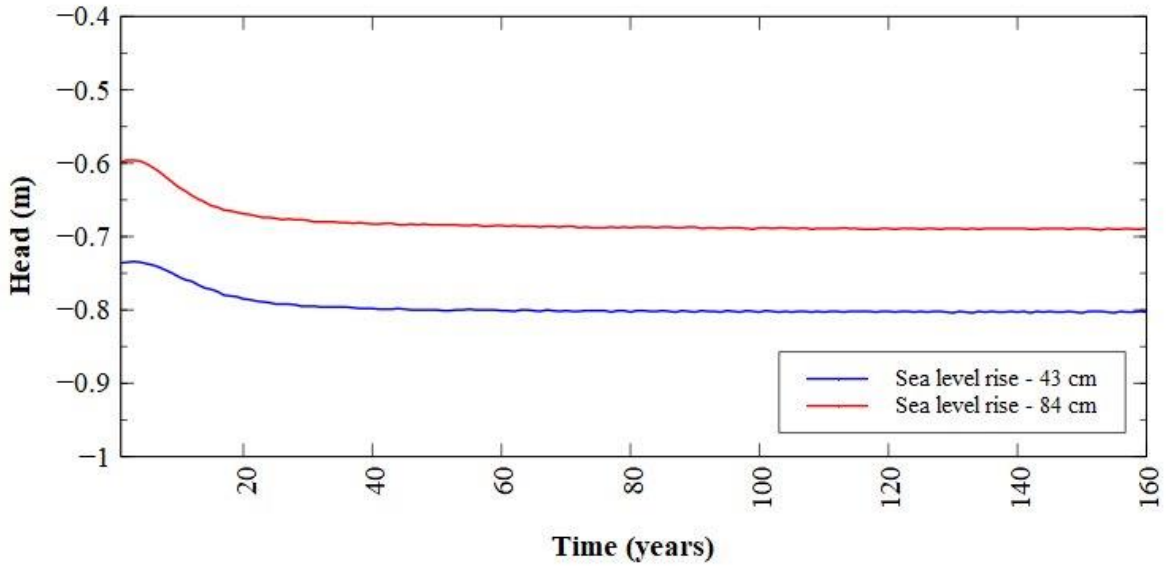

Figure 20 Change of head for piezometer D3 for sea level rise for 43 and 84 cm

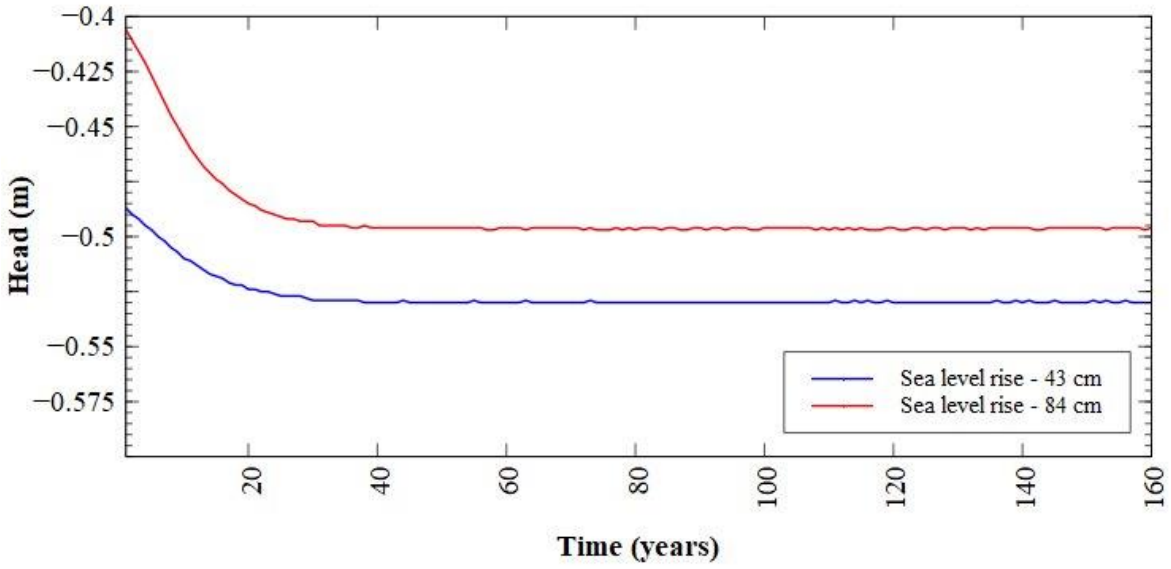

Figure 21 Change of head for piezometer D4 for sea level rise for 43 and 84 cm

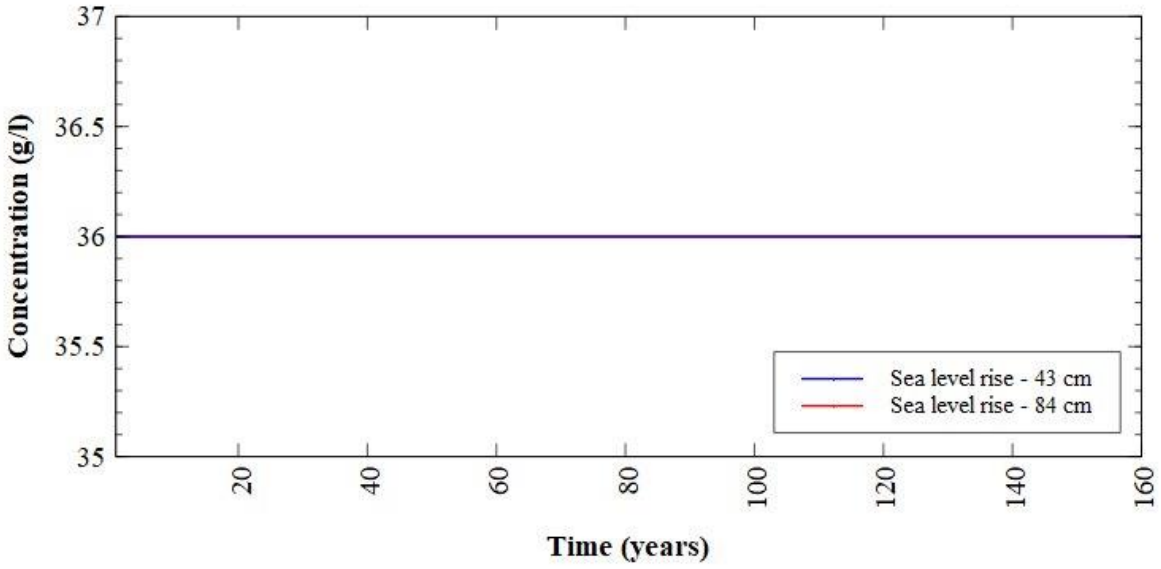

Figure 22 Change of concentration for piezometer P1 for sea level rise for 43 and 84 cm

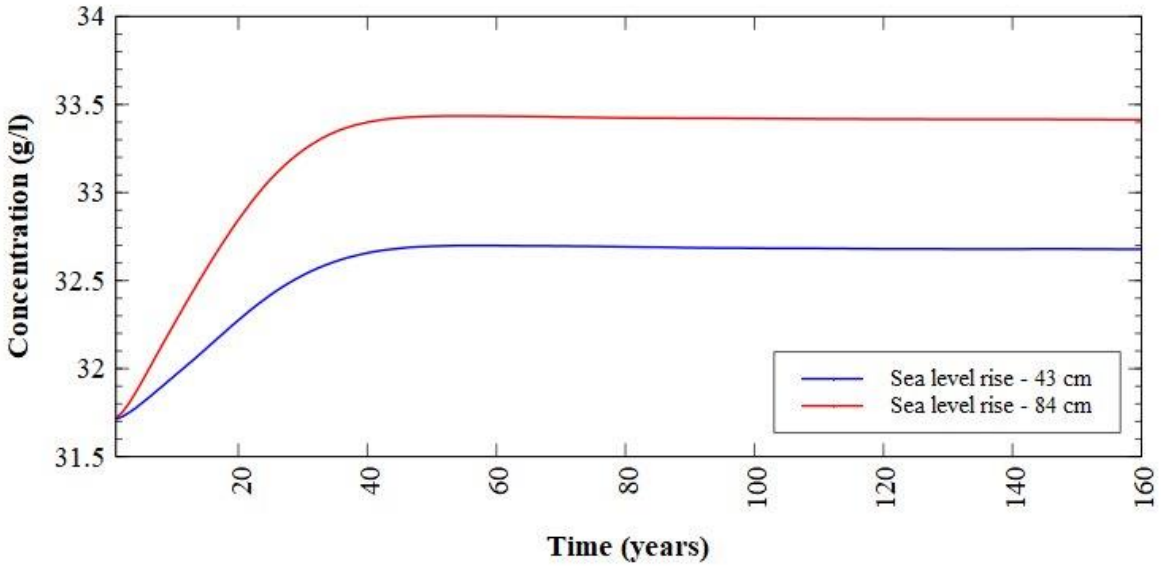

Figure 23 Change of concentration for piezometer P2 for sea level rise for 43 and 84 cm

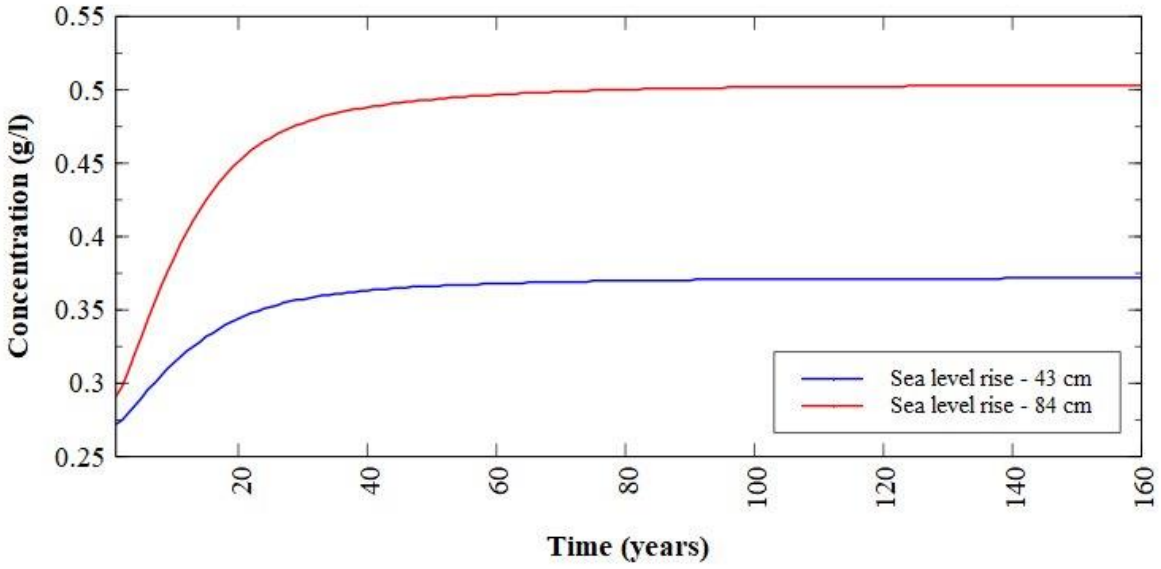

Figure 24 Change of concentration for piezometer P4 for sea level rise for 43 and 84 cm

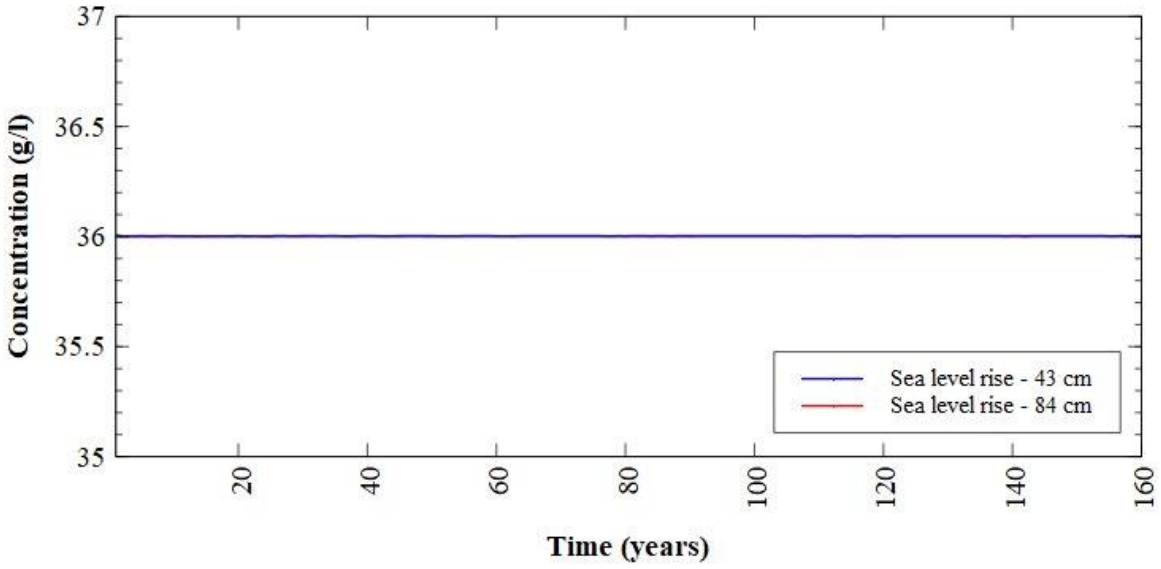

Figure 25 Change of concentration for piezometer D1 for sea level rise for 43 and 84 cm

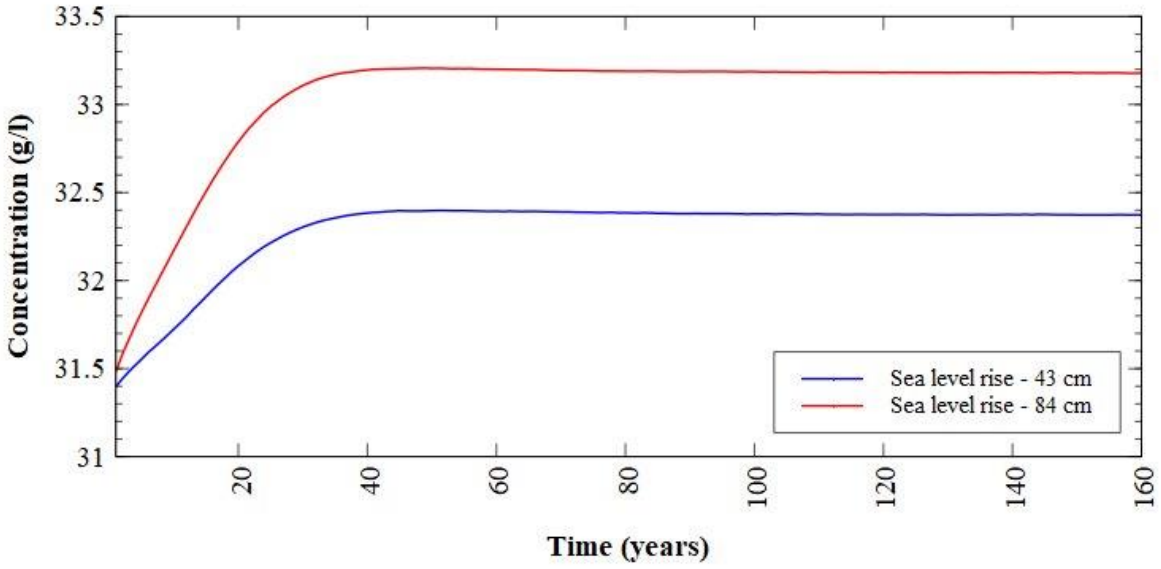

Figure 26 Change of concentration for piezometer D2 for sea level rise for 43 and 84 cm

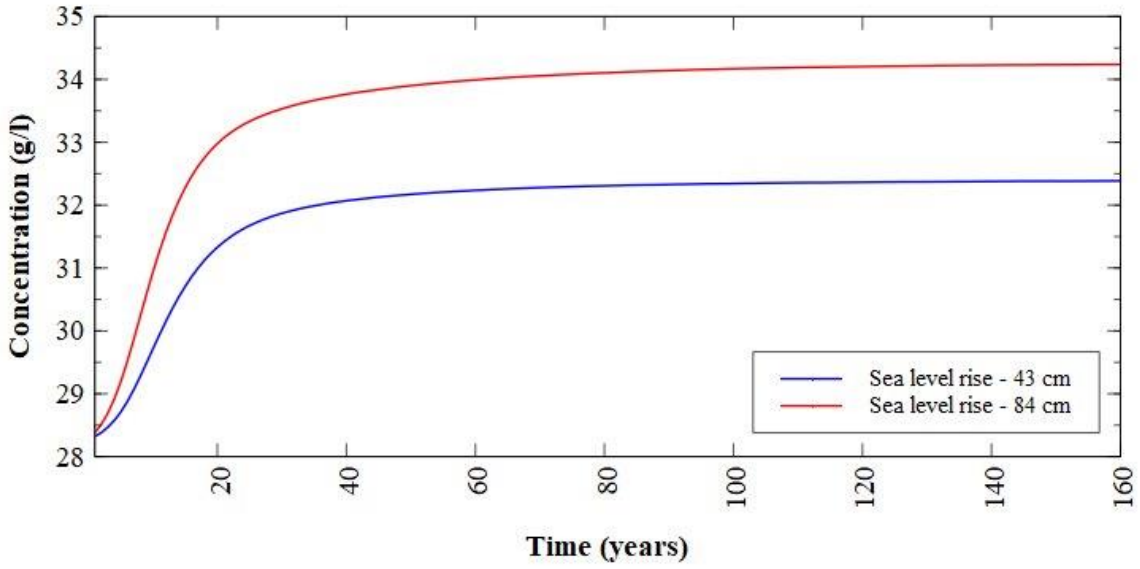

Figure 27 Change of concentration for piezometer D3 for sea level rise for 43 and 84 cm

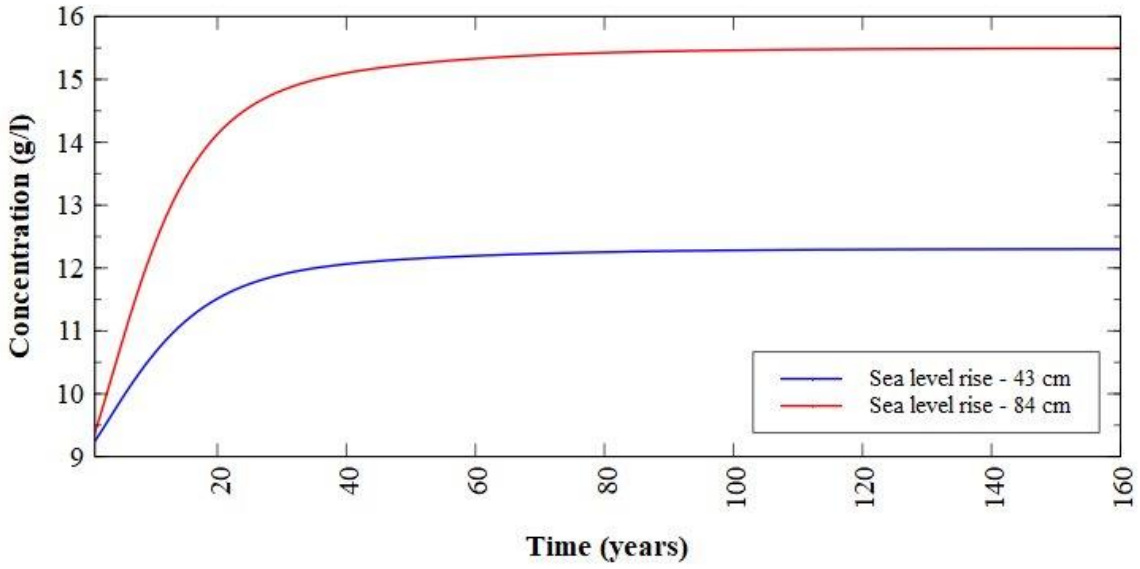

Figure 28 Change of concentration for piezometer D4 for sea level rise for 43 and 84 cm

Table 1 Change of head and concentration for all 7 locations due to sea level rise

LOCATION	Change of head for 0.43 m SLR (m)	Change of head for 0.84 m SLR (m)	Change of concentration for 0.43 m SLR (g/l)	Change of concentration for 0.84 m SLR (g/l)
P1	+0.28	+0.55	0.0	0.0
P2	+0.04	+0.07	+0.99	+1.72
P4	+0.005	+0.005	+0.1	+0.21
D1	+0.39	+0.78	0.0	0.0
D2	+0.13	+0.27	+1.0	+1.73
D3	+0.08	+0.19	+4.07	+5.86
D4	+0.04	+0.08	+3.06	+6.12

Model response due to precipitation decline

Next figures show changes in salinity field for the layer of sand and the layer of gravel due to precipitation decline. Simulations were set on flow and transport steady state simulation obtained for existing state. Simulations were set for 100 years and in that period steady state for head and for concentration is achieved for all locations.

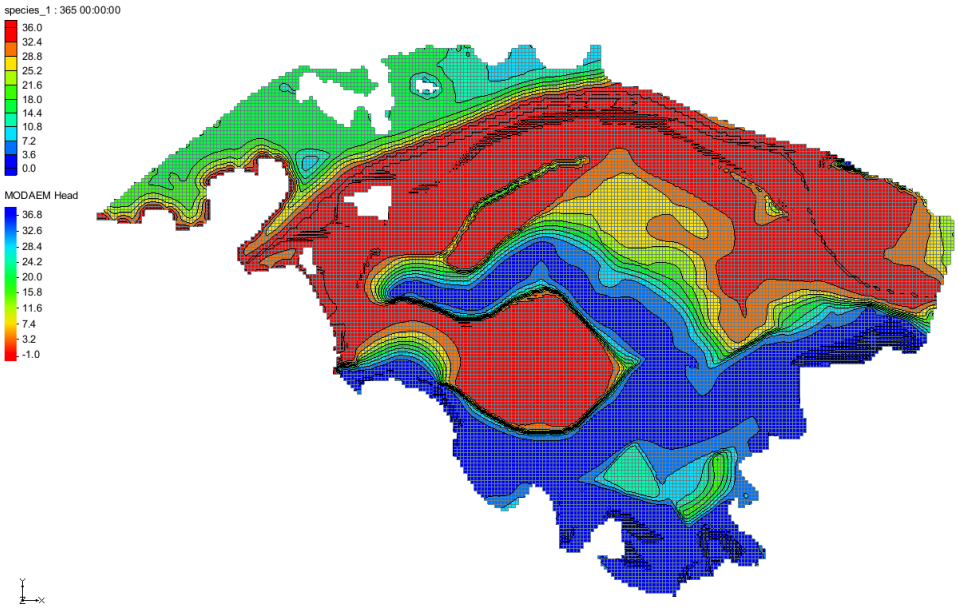

Figure 29 Salinity field for the layer of sand before climate changes

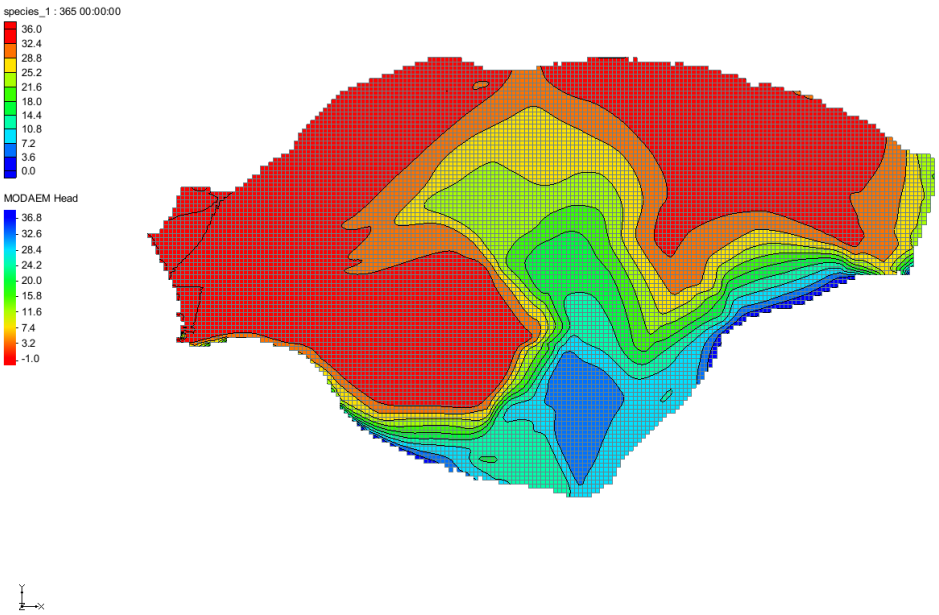

Figure 30 Salinity field for the layer of gravel before climate changes

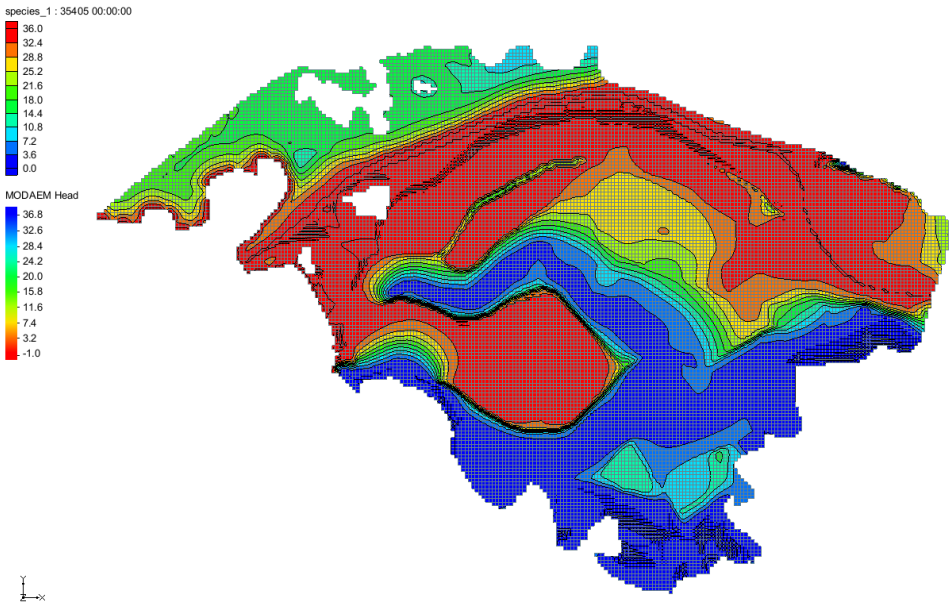

Figure 31 Salinity field for the layer of sand after 100 years of precipitation decline for 10%

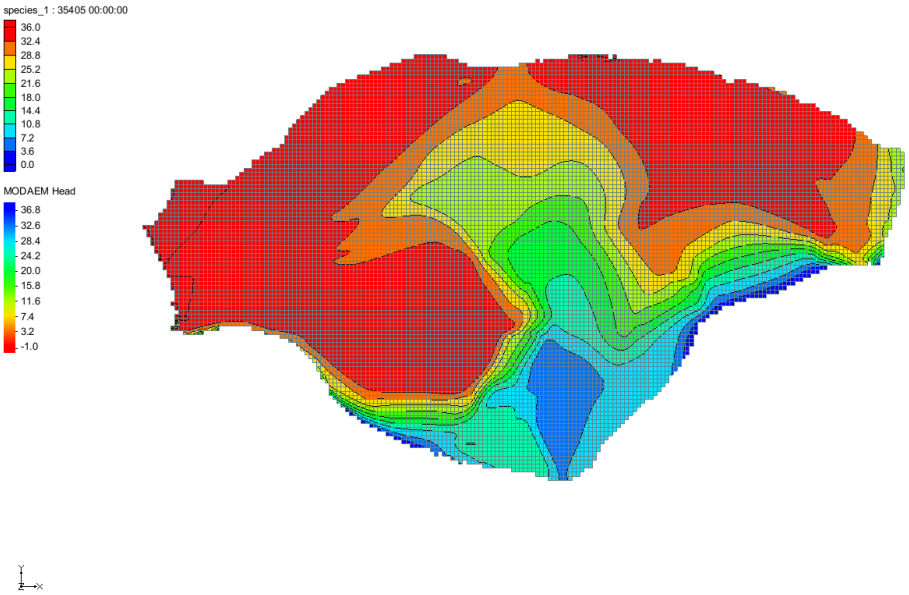

Figure 32 Salinity field for the layer of gravel after 100 years of precipitation decline for 10%

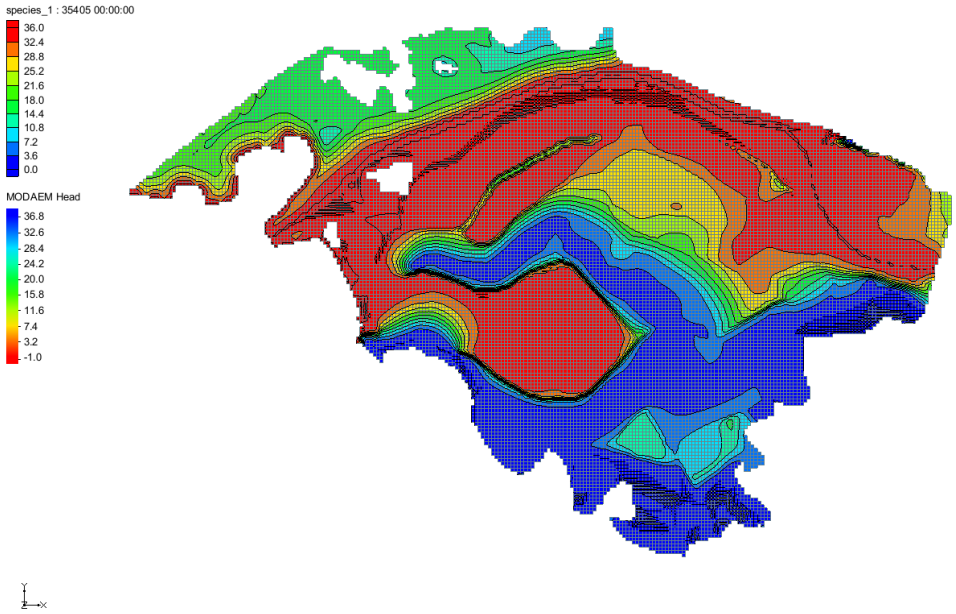

Figure 33 Salinity field for the layer of sand after 100 years of precipitation decline for 20%

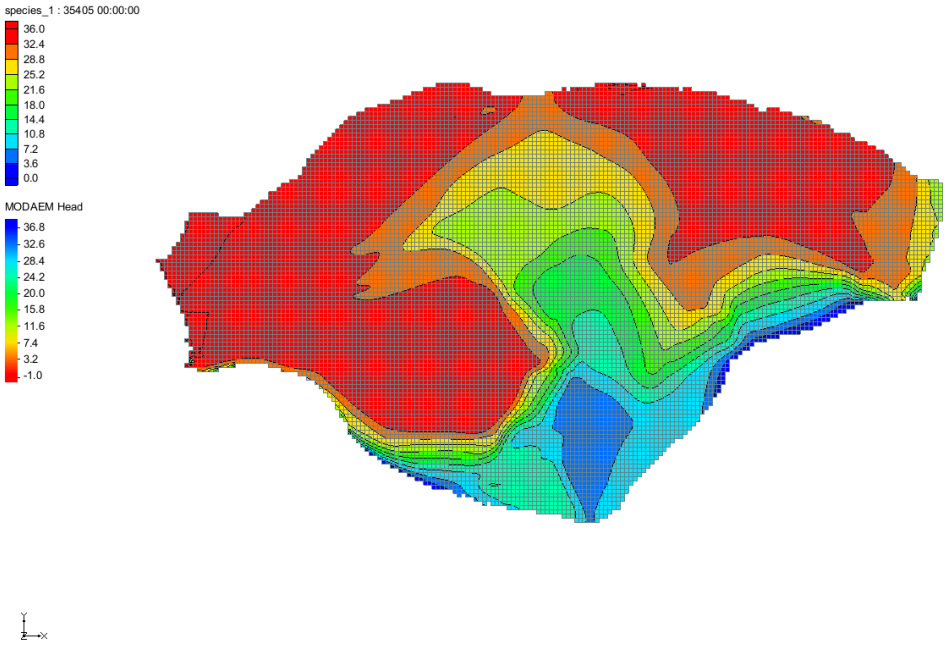

Figure 34 Salinity field for the layer of gravel after 100 years of precipitation decline for 20%

Next figures show the change of head and concentration for three shallow piezometers (P1, P2 and P4) and for four deep piezometers (D1, D2, D3 and D4) due to change in precipitation values. Simulations were set for 100 years and in that period steady state for head and for concentration is achieved for all locations.

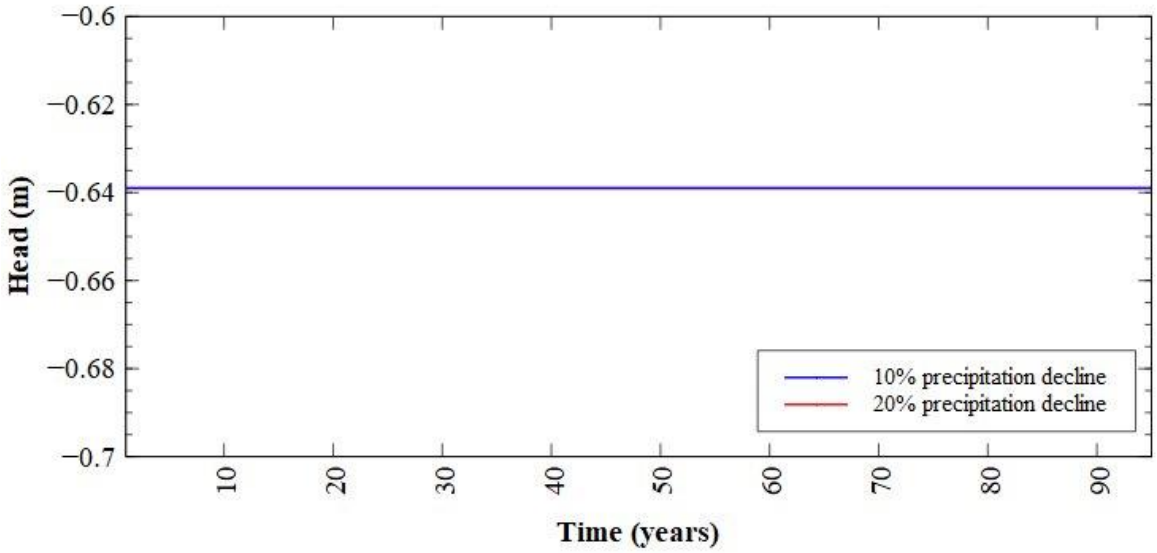

Figure 35 Change of head for piezometer P1 for precipitation decline for 10 and 20%

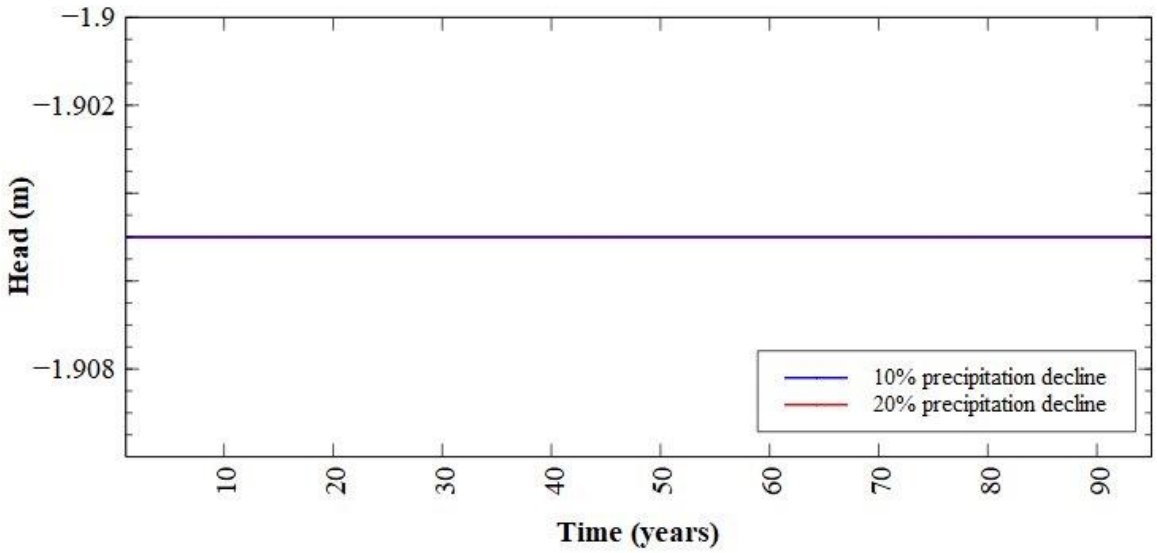

Figure 36 Change of head for piezometer P2 for precipitation decline for 10 and 20%

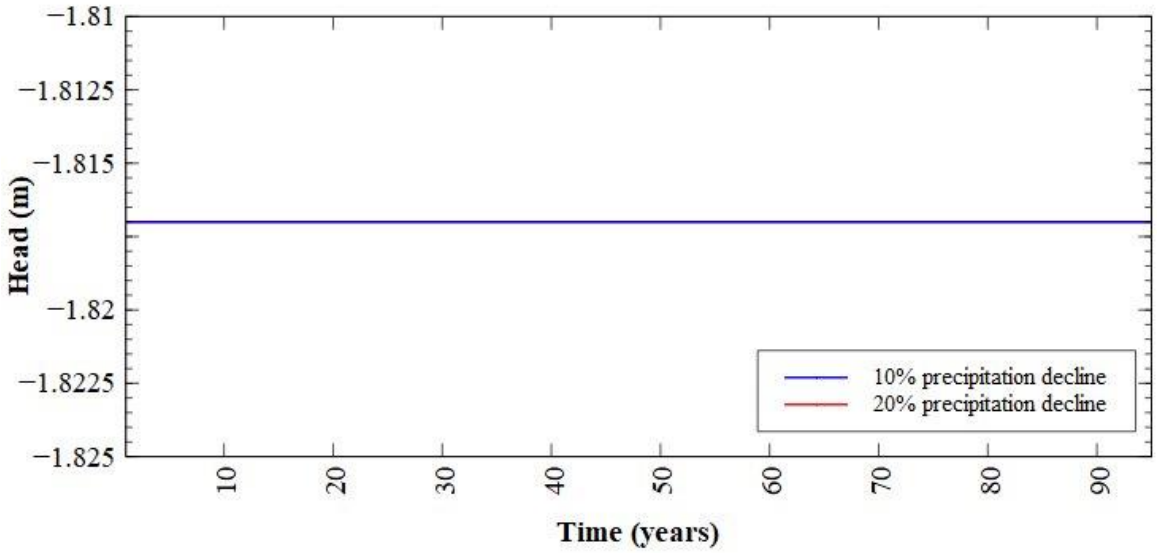

Figure 37 Change of head for piezometer P4 for precipitation decline for 10 and 20%

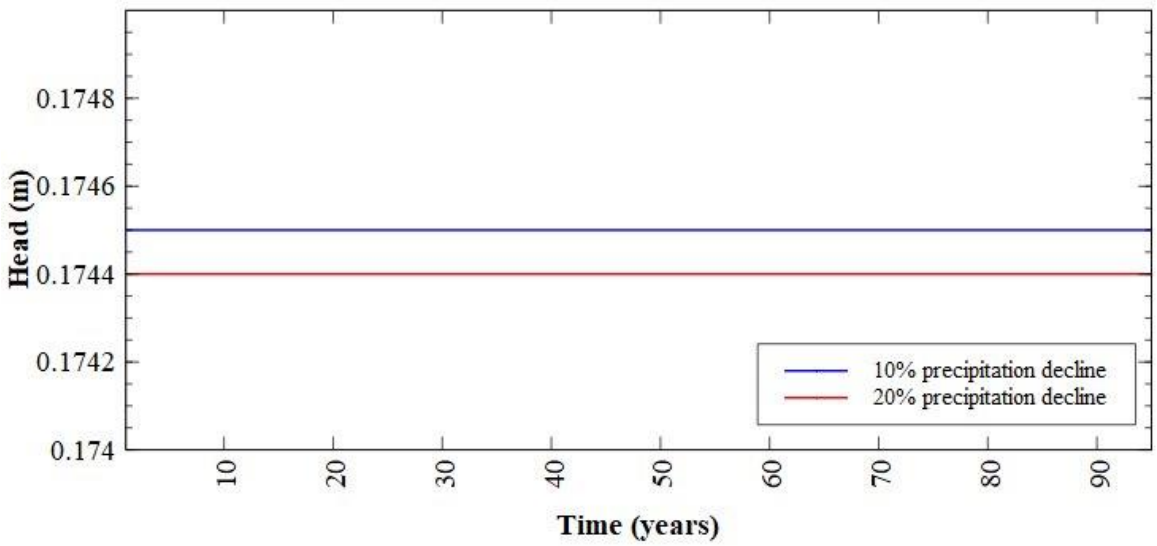

Figure 38 Change of head for piezometer D1 for precipitation decline for 10 and 20%

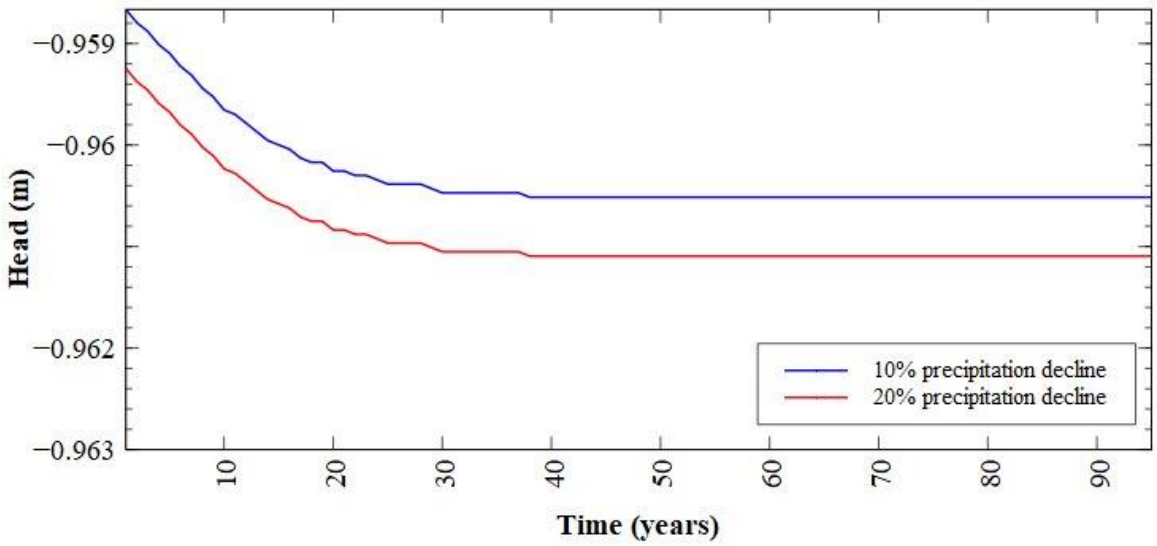

Figure 39 Change of head for piezometer D2 for precipitation decline for 10 and 20%

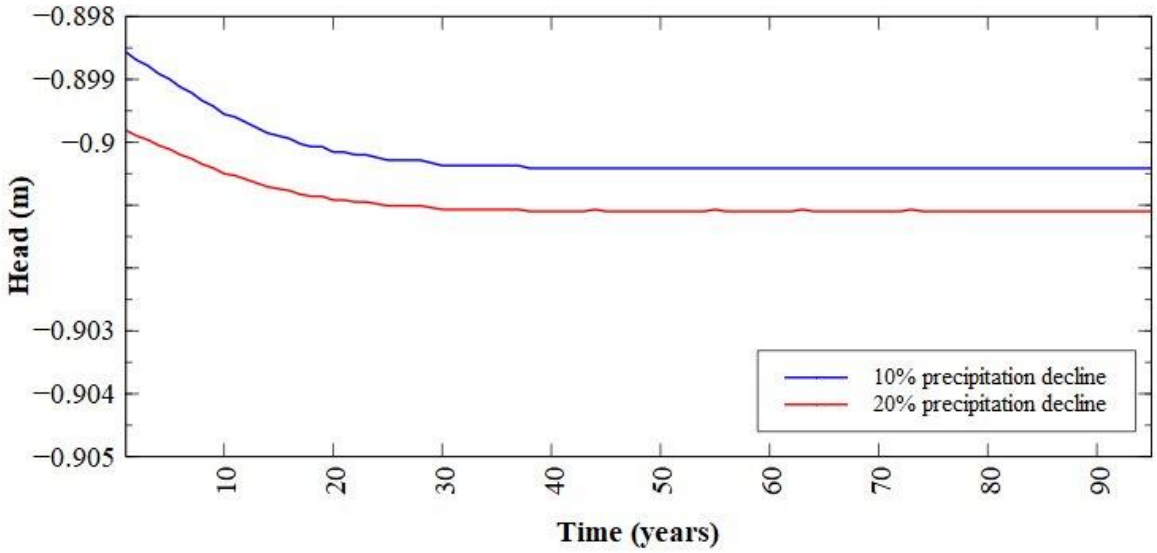

Figure 40 Change of head for piezometer D3 for precipitation decline for 10 and 20%

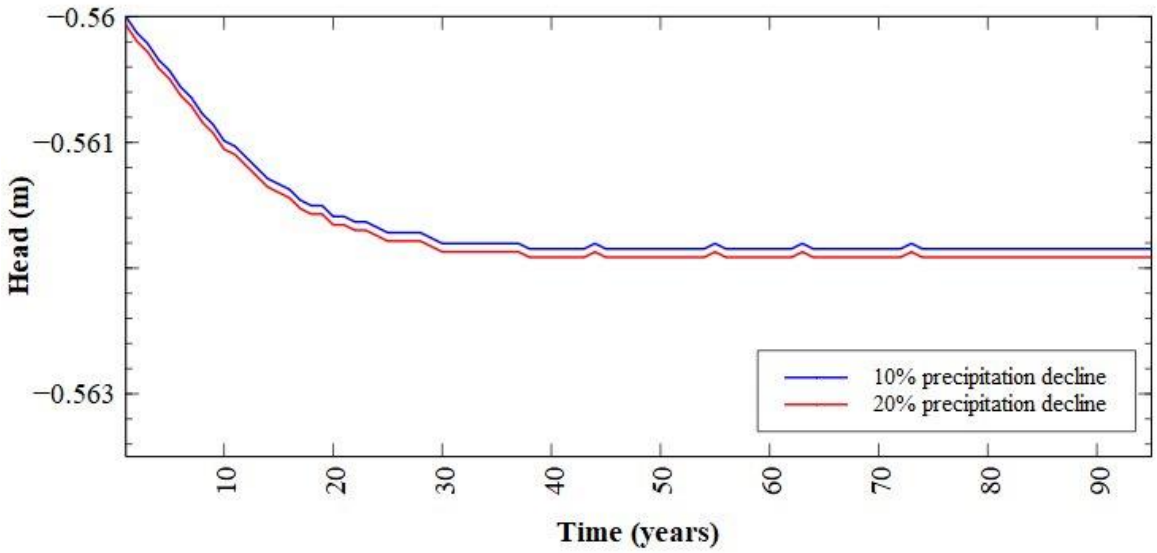

Figure 41 Change of head for piezometer D4 for precipitation decline for 10 and 20%

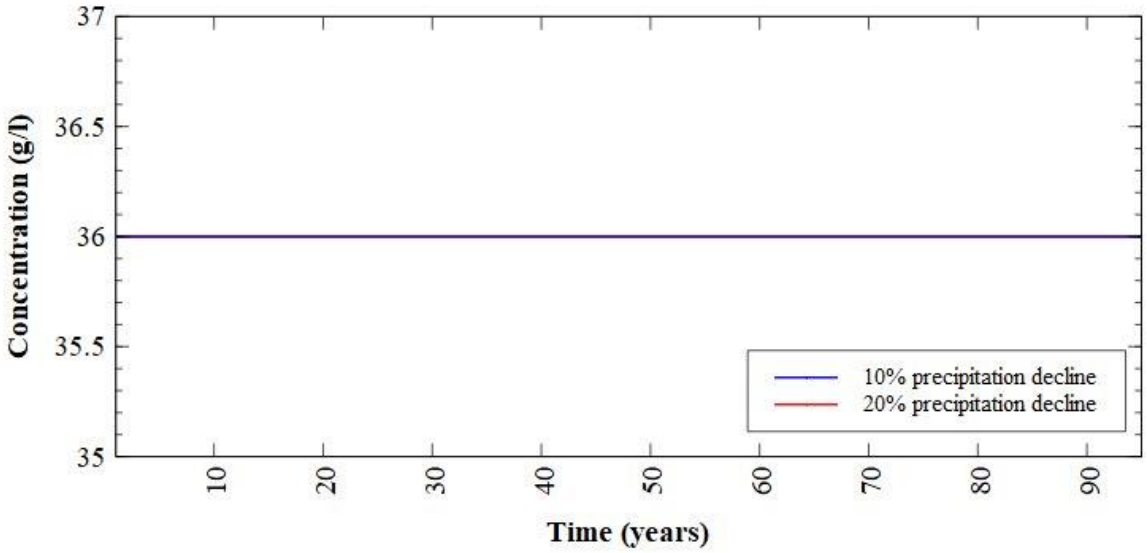

Figure 42 Change of concentration for piezometer P1 for precipitation decline for 10 and 20%

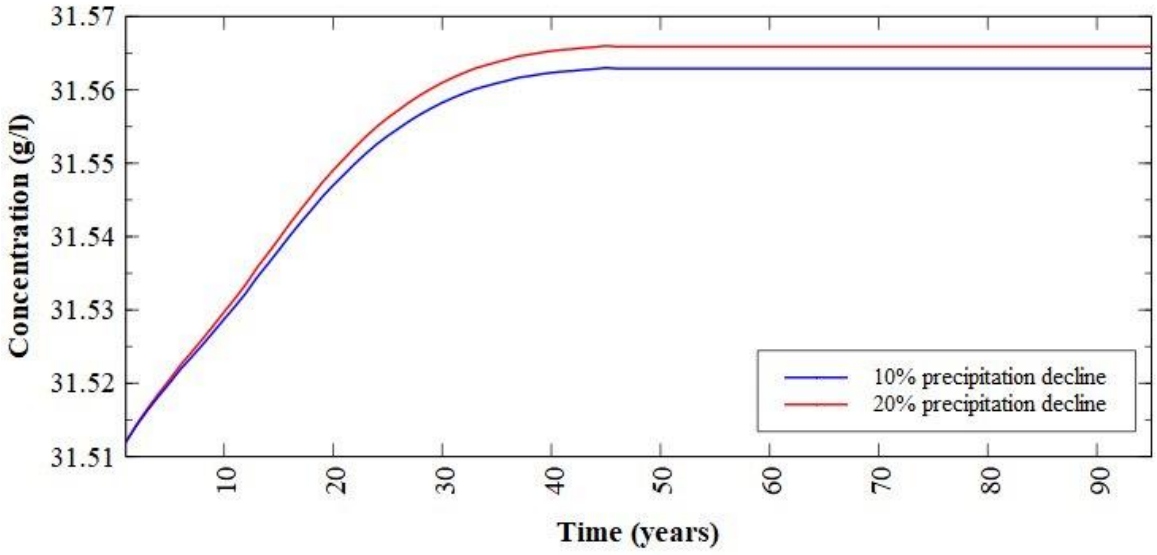

Figure 43 Change of concentration for piezometer P2 for precipitation decline for 10 and 20%

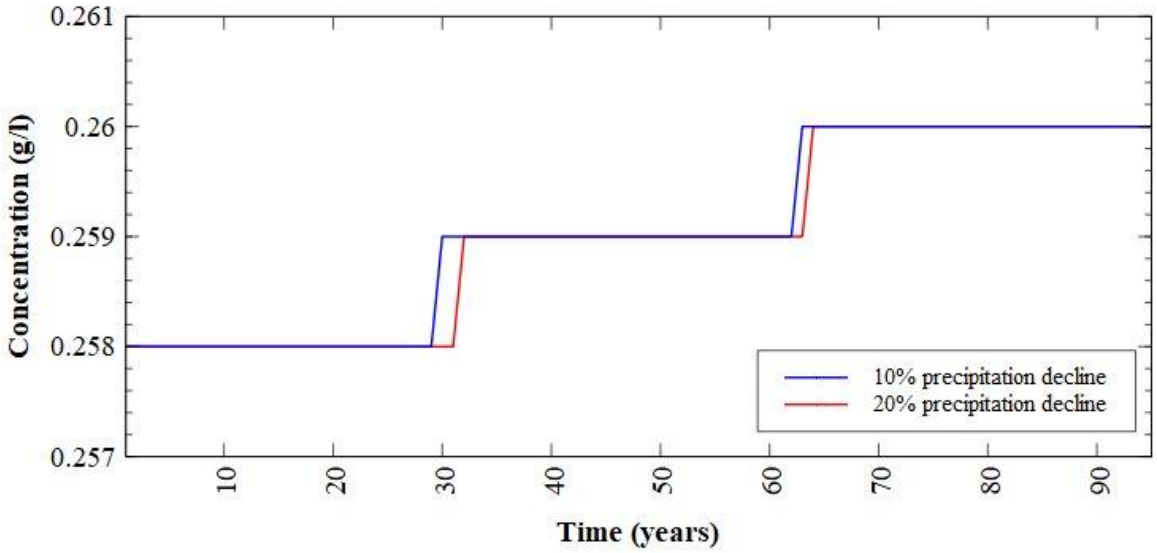

Figure 44 Change of concentration for piezometer P4 for precipitation decline for 10 and 20%

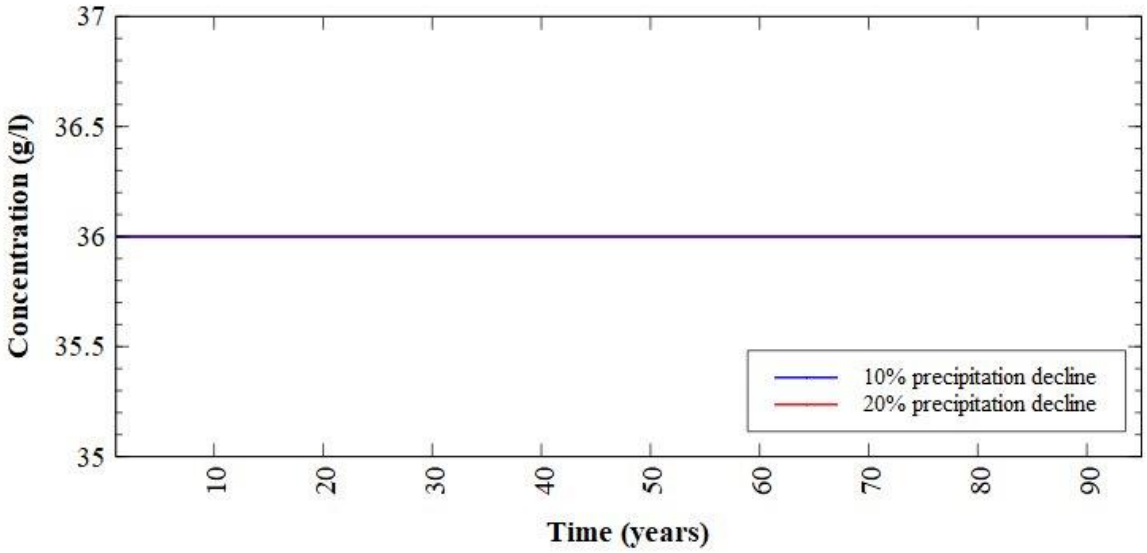

Figure 45 Change of concentration for piezometer D1 for precipitation decline for 10 and 20%

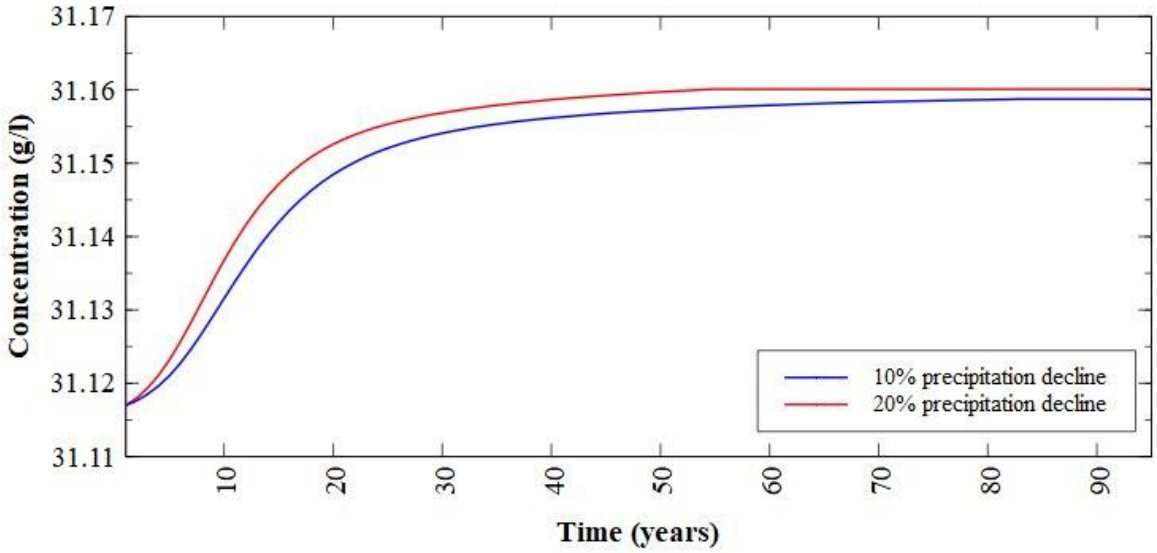

Figure 46 Change of concentration for piezometer D2 for precipitation decline for 10 and 20%

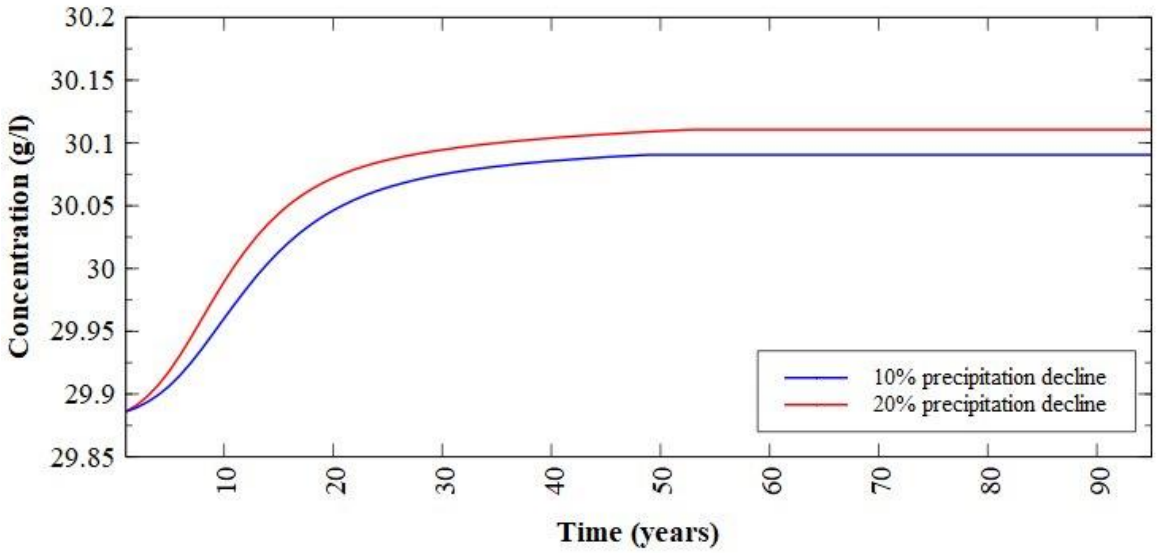

Figure 47 Change of concentration for piezometer D3 for precipitation decline for 10 and 20%

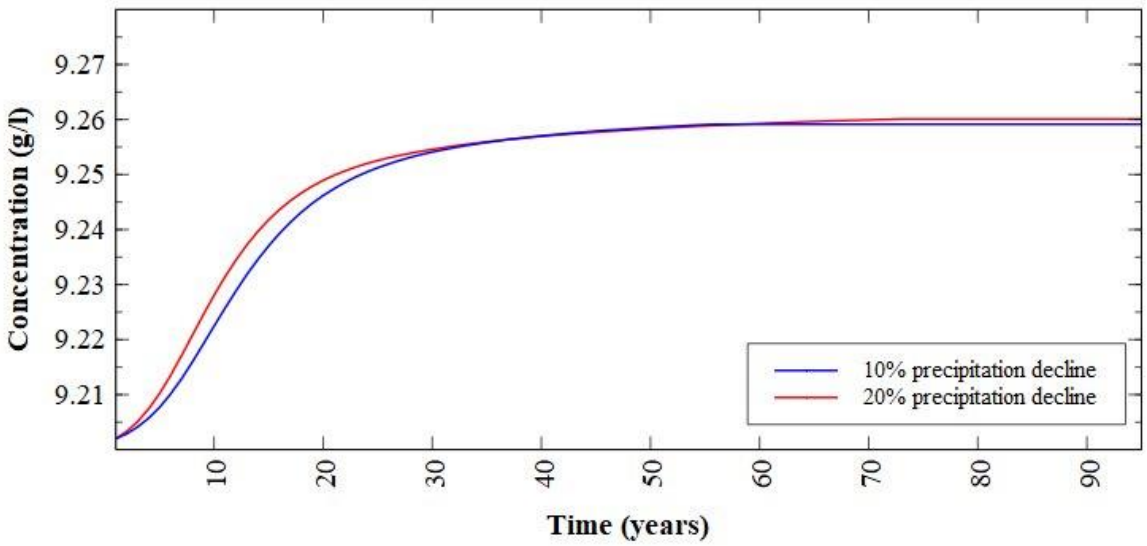

Figure 48 Change of concentration for piezometer D4 for precipitation decline for 10 and 20%

Table 2 Change of head and concentration for all 7 locations due to precipitation decline

LOCATION	Change of head for 10% precipitation decline (m)	Change of head for 20% precipitation decline (m)	Change of concentration for 10% precipitation decline (g/l)	Change of concentration for 20% precipitation decline (g/l)
P1	0.0	0.0	0.0	0.0
P2	-0.001	-0.001	+0.0051	+0.0054
P4	0.0	0.0	+0.002	+0.002
D1	0.0	-0.002	0.0	0.0
D2	-0.005	-0.004	+0.0013	+0.0013
D3	-0.003	-0.003	+0.002	+0.002
D4	-0.002	-0.002	+0.001	+0.001

Mitigation measures

Three mitigation measures scenarios suitable for River Neretva Valley were proposed and tested in the model. Those scenarios are:

- Impermeable underground barrier below Diga embankment
- Barrier on River Neretva near Komin
- Barrier on River Neretva near Komin with channel parallel with River Neretva

Figure 49 shows location of underground barrier below Diga, barrier on River Neretva and existing channel parallel with River Neretva used as source of fresh water in combination with barrier on River Neretva.

Figure 49 Location of elements for mitigation measures

Impermeable underground barrier below Diga embankment (M1)

Impermeable underground barrier below Diga embankment is the first mitigation measure tested in the model. Main idea behind this mitigation measure is that impermeable underground barrier should prevent salt water intrusion below Diga embankment. Impermeable underground barrier was located from the River Neretva on northwest up to pumping station Modrič on southeast, below Diga embankment.

Since Diga embankment is artificially made embankment constructed in 1960s it is made out of different kind of material than the rest of the valley. The model of existing state adopted higher values for hydraulic conductivity for the area of Diga embankment and defined it as more permeable area.

Mitigation measure scenario M1 was tested as steady state (transient constant) simulation set for the period of 160 years.

Flow boundary conditions for mitigation measure M1 simulation were mean values of boundary condition determined for existing state simulations. Flow initial condition for mitigation measure M1 simulation were head results of flow steady state simulation.

Transport boundary conditions for mitigation measure M1 simulation were concentration value of 36 g/l along the sea line and in River Neretva. Boundary conditions for Opuzen, Mala Neretva and channels were defined as $dC/cX \neq 0$, $dC/dZ \neq 0$. Transport initial condition for mitigation measure M1 simulation were the values of concentration obtained in flow and transport steady state simulation.

For simulation of impermeable underground barrier below Diga embankment the material of clay was used. Material was set along the whole area of Diga embankment in the first five layers of the model. All geological characteristics of the clay were used with the value of horizontal hydraulic conductivity 10^{-9} m/s.

Figure 50 shows the values of horizontal hydraulic conductivity in the layer of sand set for mitigation measure M1.

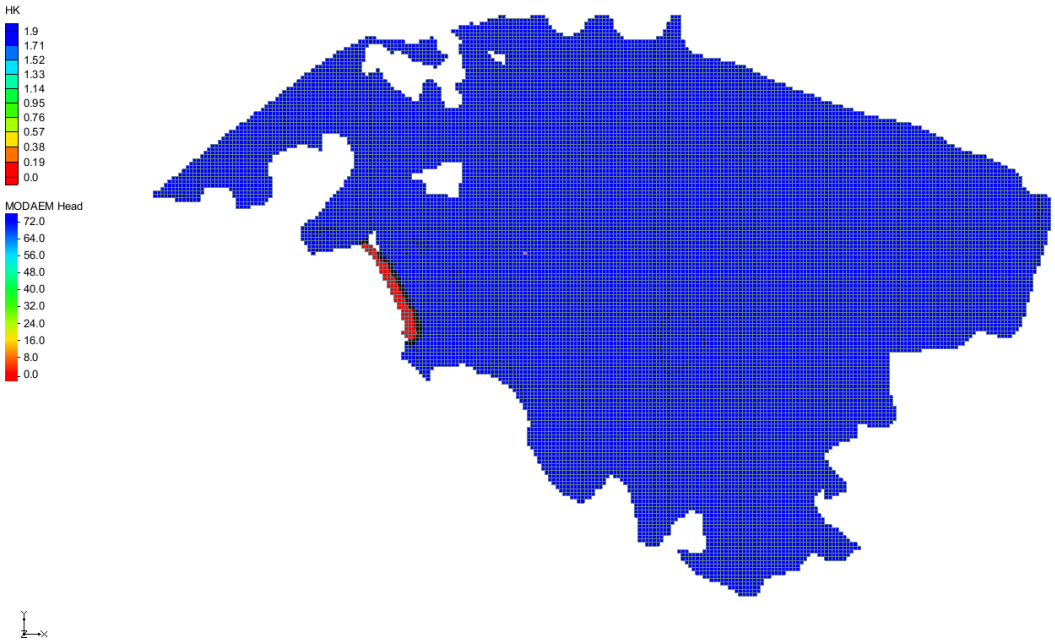

Figure 50 Values of horizontal hydraulic conductivity in the layer of sand for mitigation measure M1

Barrier on River Neretva near Komin (M2)

Barrier on River Neretva near Komin is the second mitigation measure tested in the model.

Since the salt water wedge is noticed in all samplings taken on River Neretva (near Komin and Opuzen) during summer period it was possible to conclude that River Neretva is a source of salt water during the summer period. Main idea behind this mitigation measure is that barrier on River Neretva near Komin should prevent salt water intrusion trough river Neretva during the summer period. The barrier should also increase water level in River Neretva upstream from the barrier for 30 cm. In case of implementation of the barrier, River Neretva (with its increased level of fresh water upstream from the barrier) would serve as source of fresh water available for irrigation.

Mitigation measure scenario M2 was tested as steady state (transient constant) simulation set for the period of 160 years.

Flow boundary conditions for mitigation measure M2 simulation were mean values of all boundary condition determined for existing state simulations. The only exception was boundary condition for River Neretva upstream from barrier near Komin. Head values in the River Neretva upstream from the barrier were elevated for 30 cm based on estimated level of increase. Flow initial condition for mitigation measure M2 simulation were head results of flow steady state simulation.

Transport boundary conditions for mitigation measure M2 simulation were concentration value of 36 g/l along the sea line. Boundary conditions for Opuzen, Mala Neretva and channels were defined as $dC/cX \neq 0$, $dC/dZ \neq 0$. Transport initial condition for mitigation measure M2 simulation were the values of concentration obtained in flow and transport steady state simulation.

Transport boundary conditions for River Neretva was set as concentration value of 36 g/l up to barrier near Komin and as concentration value of 0 g/l upstream from barrier near Komin.

Barrier on River Neretva near Komin with channel parallel with River Neretva (M3)

Barrier on River Neretva near Komin with channel parallel with River Neretva is the third mitigation measure tested in the model and it is based on second mitigation measure scenario. Main idea behind this mitigation measure is that barrier on River Neretva near Komin should increase level of fresh water upstream from the barrier witch is possible to use as a source of fresh water for channel parallel with River Neretva. With barrier on River Neretva near Komin and channel parallel with River Neretva the greater part of the valley has access to fresh water during the whole year.

Mitigation measure scenario M3 was tested as steady state (transient constant) simulation set for the period of 160 years.

Flow boundary conditions for mitigation measure M3 simulation were mean values of all boundary condition determined for existing state simulations. The only exception was boundary condition for River Neretva upstream from barrier near Komin. Head values in the River Neretva upstream from the barrier were elevated for 30 cm based on estimated level of increase. Flow initial condition for mitigation measure M3 simulation were head results of flow steady state simulation.

Transport boundary conditions for mitigation measure M3 simulation were concentration value of 36 g/l along the sea line. Boundary conditions for Opuzen, Mala Neretva and channels were defined as $dC/cX \neq 0$, $dC/dZ \neq 0$. Transport initial condition for mitigation measure M3 simulation were the values of concentration obtained in flow and transport steady state simulation.

Transport boundary conditions for River Neretva was set as concentration value of 36 g/l up to barrier near Komin and as concentration value of 0 g/l upstream from barrier near Komin. Transport boundary conditions for channel parallel with River Neretva and used as a source of fresh water was set with a concentration value of 0 g/l.

Figure 51 shows transport boundary conditions set for mitigation measure M3.

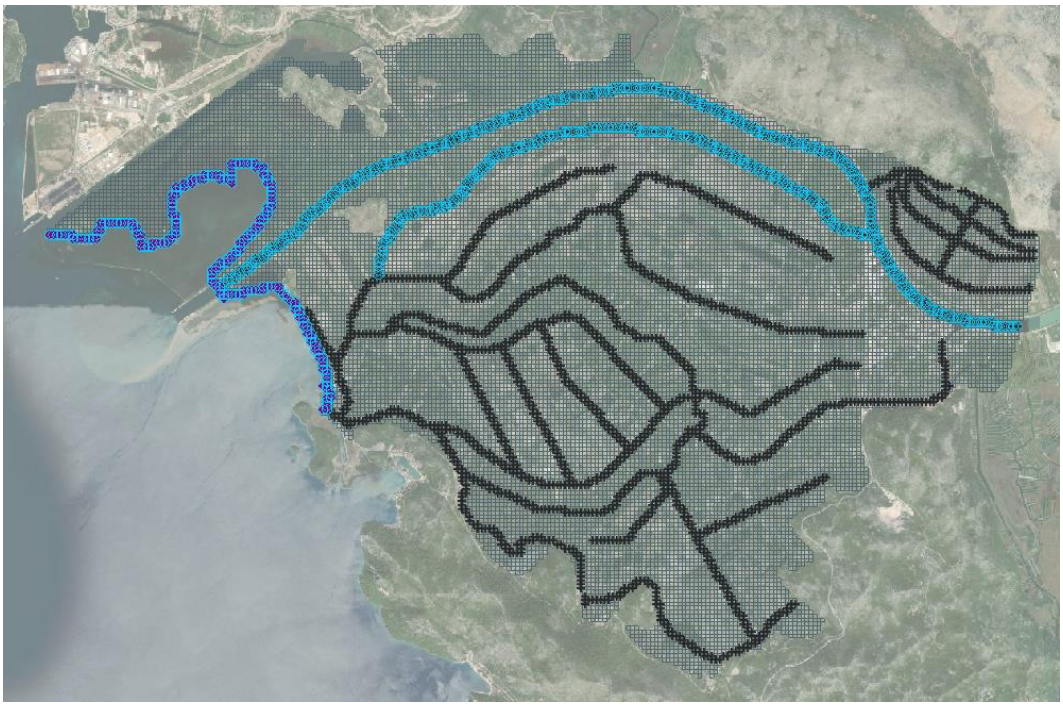

Figure 51 Transport boundary conditions for mitigation measure M3

Model application of mitigation strategies for the selected scenarios of climate changes

Results for all mitigation measures are shown on next figures. Results are shown only for surface layer since the purpose of mitigation measures is to prevent salt water intrusion and improve conditions for agriculture. Since head distribution is connected with channel regime and it is under small influence of climate changes in surface layer, only salinity distribution is shown.

Mitigation measures are marked as follows:

- Impermeable underground barrier below Diga embankment – M1
- Barrier on River Neretva near Komin – M2
- Barrier on River Neretva near Komin with channel parallel with River Neretva – M3

Figure 52 to Figure 55 present transport initial state for mitigation measure scenarios. This salinity fields are result of steady state simulations obtained for climate change scenarios.Figure 52 Salinity field in the layer of sand for SLR for 43 cm

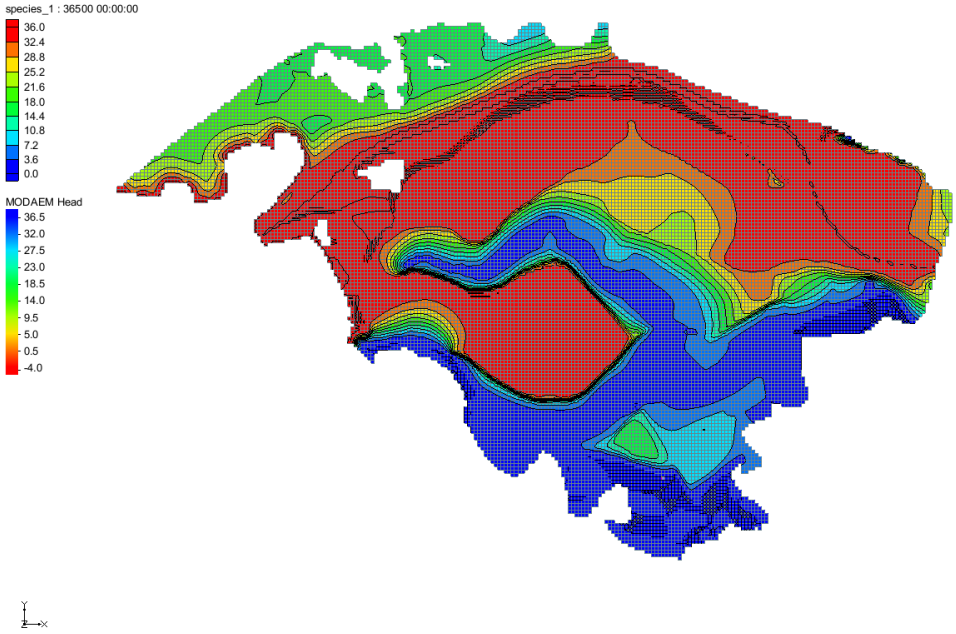

Figure 52 Salinity field in the layer of sand for SLR for 43 cm

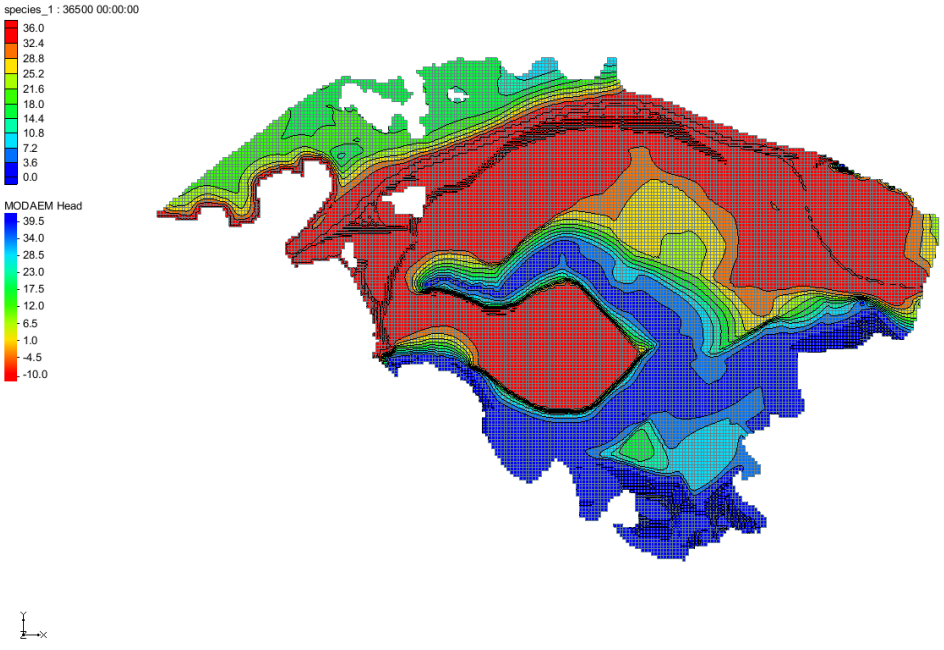

Figure 53 Salinity field in the layer of sand for SLR for 84 cm

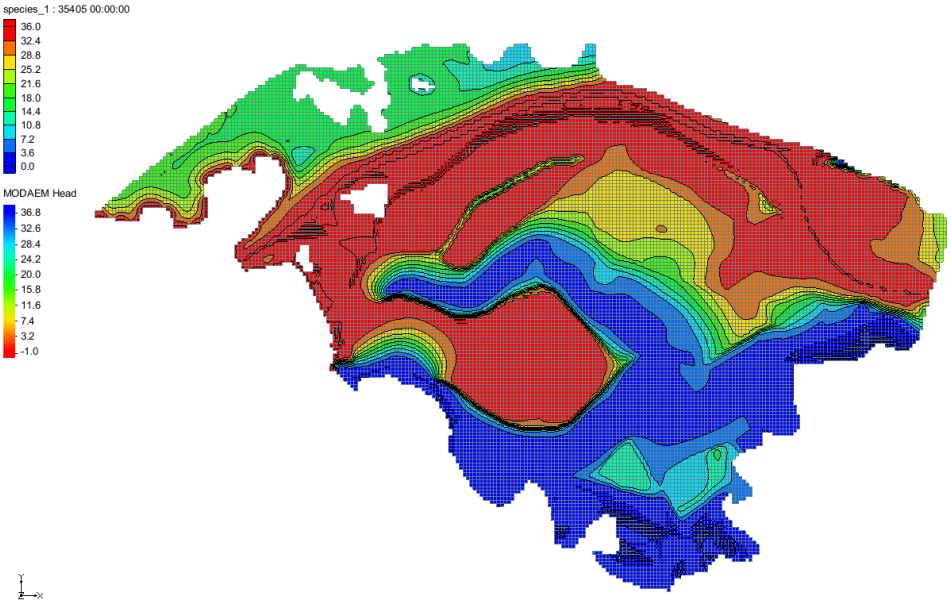

Figure 54 Salinity field in the layer of sand for precipitation decline for 10%

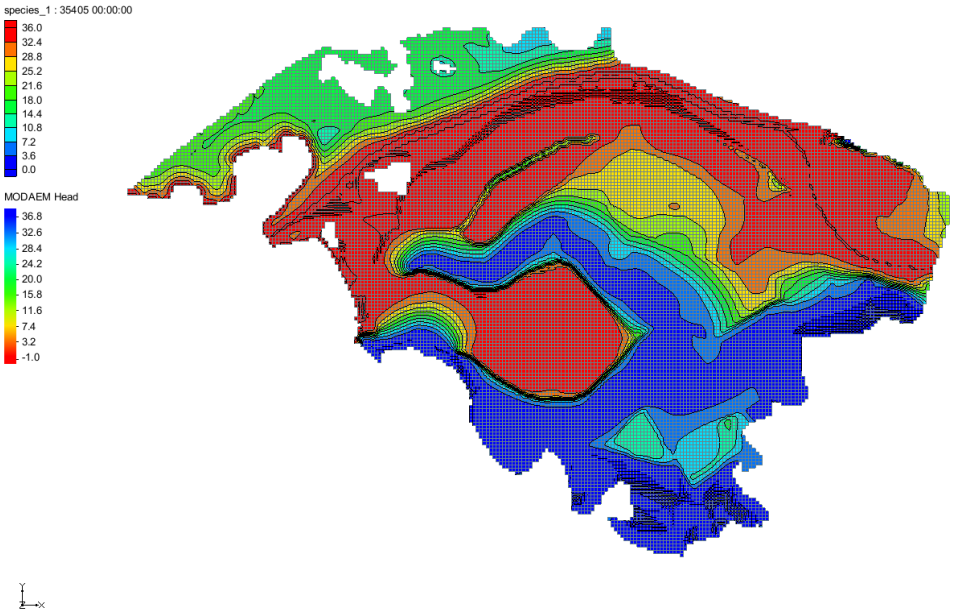

Figure 55 Salinity field in the layer of sand for precipitation decline for 20%

Changes in head and concentration for all piezometer location due to selected climate change scenarios are numerically shown in Table 1 and Table 2. Based on the figures presenting climate change final results, it is possible to conclude that changes in head and concentration for all climate change scenarios and on all locations shown on the model scale look quite similar.

Next figures present salinity fields for different mitigation measures after 1 and 160 years. Since the figures for different climate change scenarios look quite similar, only representative figures are presented.

Exact values for different climate change and locations are shown in next chapter.

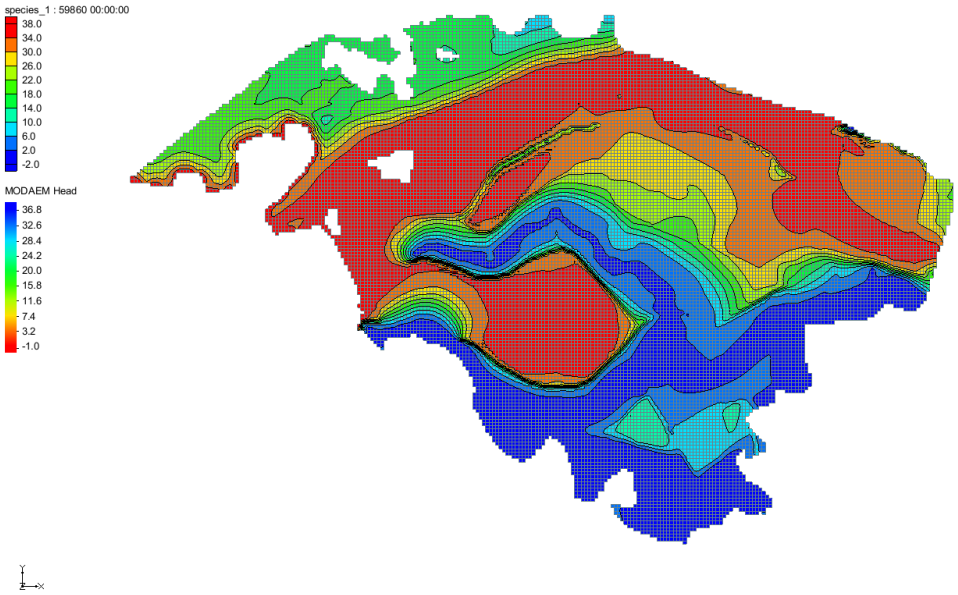

Figure 56 Salinity field for the layer of sand after 160 years due to mitigation measure M1

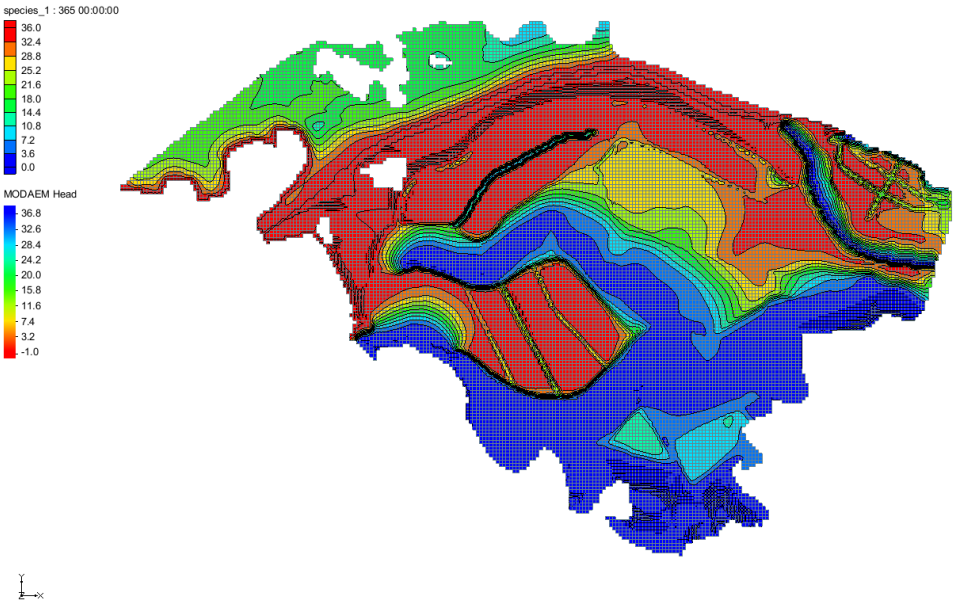

Figure 57 Salinity field for the layer of sand after 1 year due to mitigation measure M2

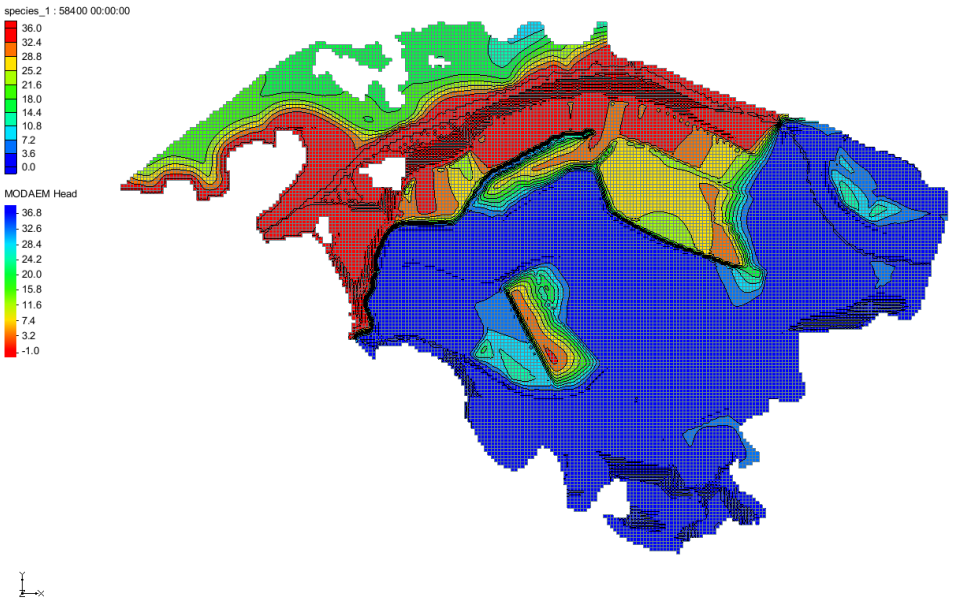

Figure 58 Salinity field for the layer of sand after 160 years due to mitigation measure M2

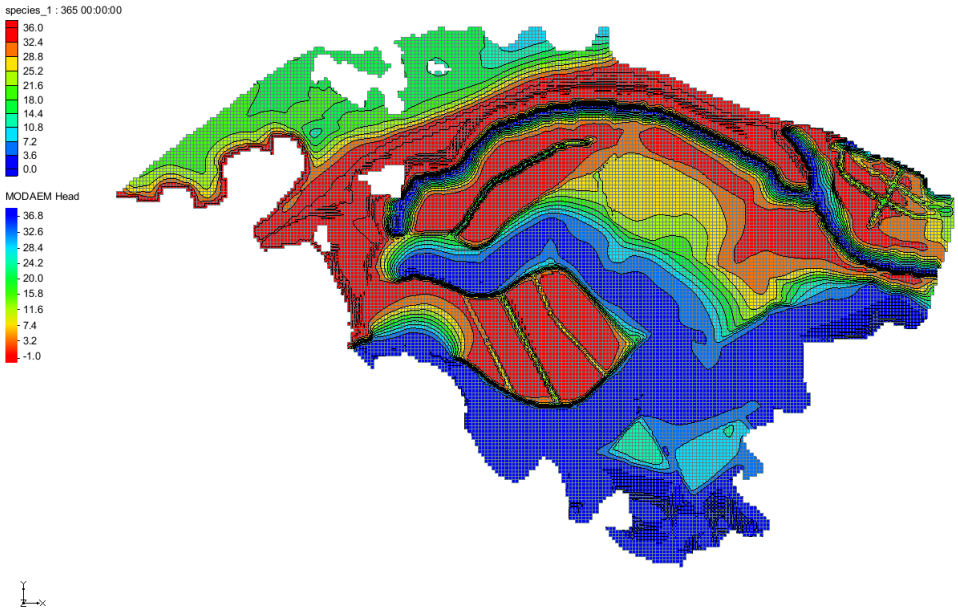

Figure 59 Salinity field for the layer of sand after 1 year due to mitigation measure M3

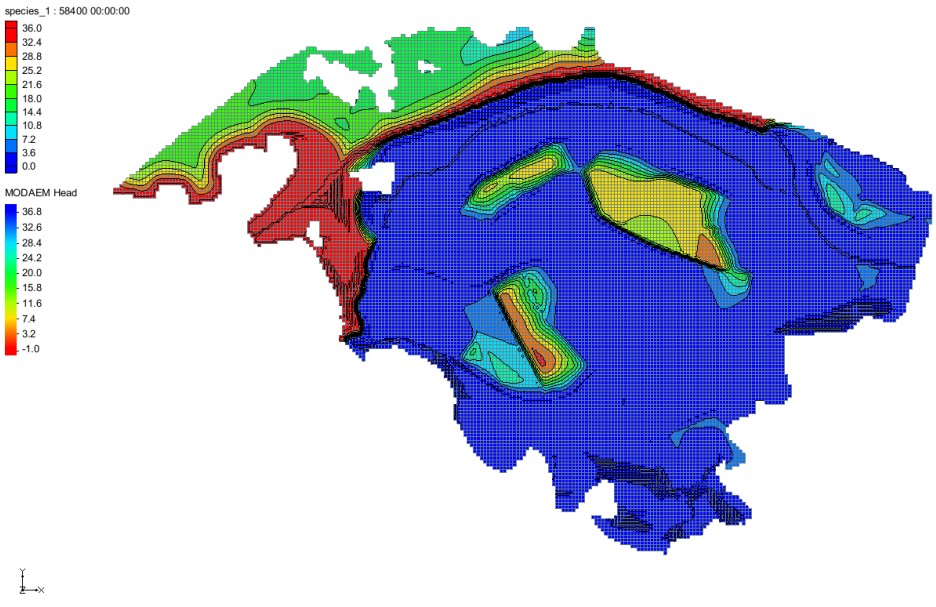

Figure 60 Salinity field for the layer of sand after 160 years due to mitigation measure M3

The efficiency of mitigation strategies for the selected scenarios of climate changes

On the next figures change of concentration values is shown for three shallow piezometers due to mitigation measures for scenarios after climate changes. Period of 160 years is shown and in that period steady state is established in all locations.

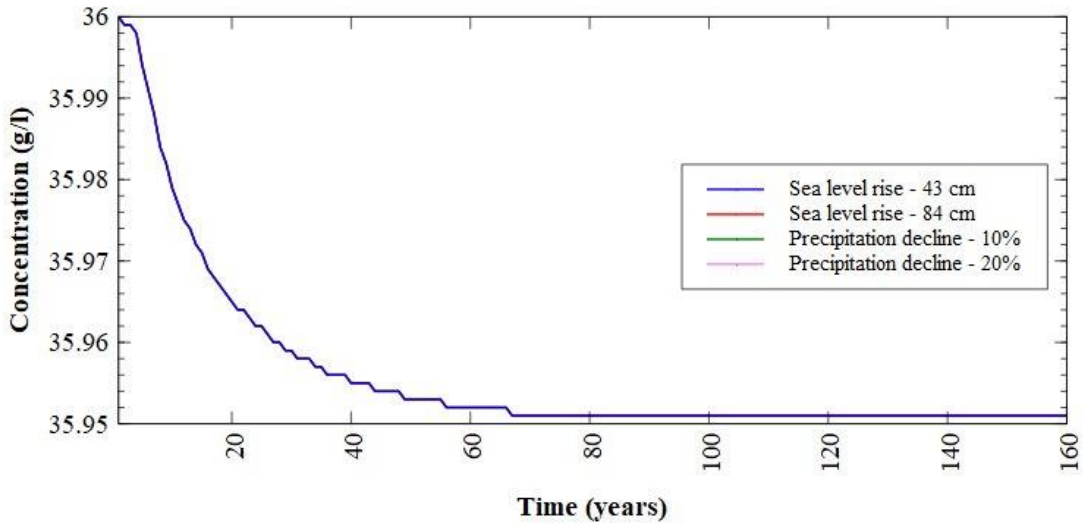

Figure 61 Change of concentration for piezometer P1 for mitigation measure M1 after climate changes

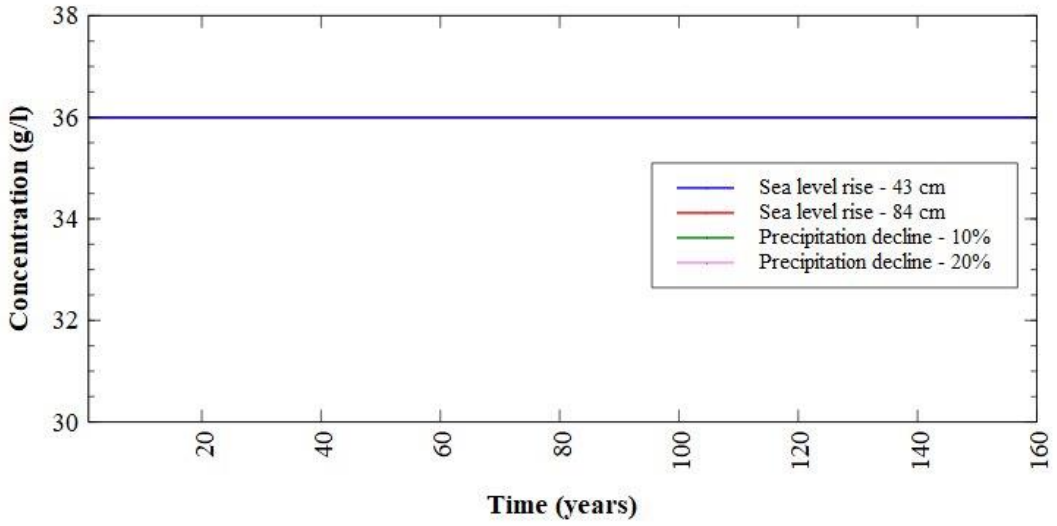

Figure 62 Change of concentration for piezometer P1 for mitigation measure M2 after climate changes

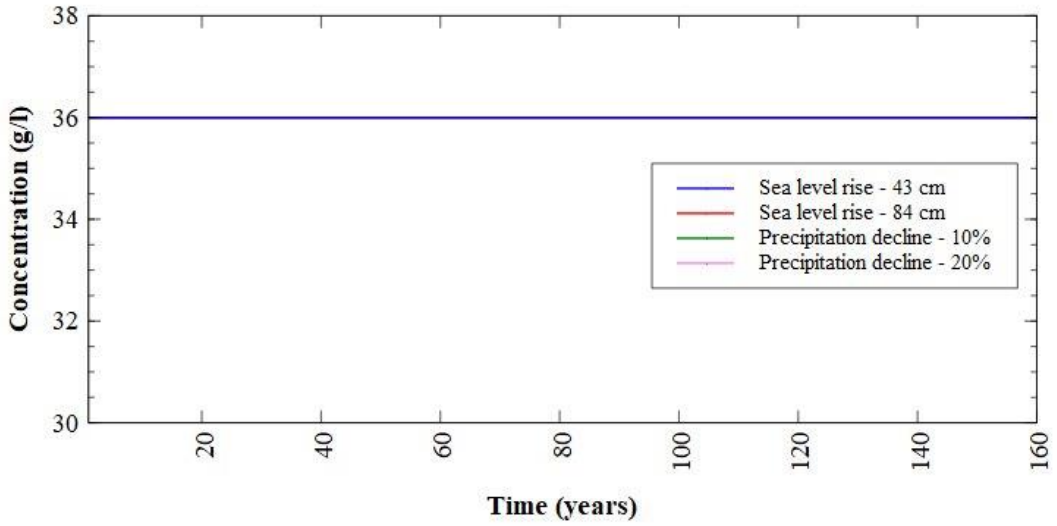

Figure 63 Change of concentration for piezometer P1 for mitigation measure M3 after climate changes

Table 3 Change of concentration and time needed to achieve steady state on location P1 for all mitigation measures after climate changes

		Mitigation measure M1	Mitigation measure M2	Mitigation measure M3
Change of concentration (g/l)	0.43 m SLR	-0.05	0	0
	0.84 m SLR	-0.05	0	0
	10% precipitation decline	-0.05	0	0
	20% precipitation decline	-0.05	0	0
Time needed to achieve steady state (years)	0.43 m SLR	67	0	0
	0.84 m SLR	67	0	0
	10% precipitation decline	67	0	0
	20% precipitation decline	67	0	0

Based on Figure 61 to Figure 63 and Table 3 it is possible to conclude that changes of concentration values on location P1 are quite small. The only mitigation measure that shows any effect at lowering concentration values is mitigation measure M1 (impenetrable underground barrier bellow Diga embankment). Mitigation measure M1 lowers concentration value for 0.05 g/l during the period of 67 years after all climate changes. The reason for low efficiency of mitigation measures on lowering concentration on location P1 is its vicinity to the sea and permeability of Diga embankment.

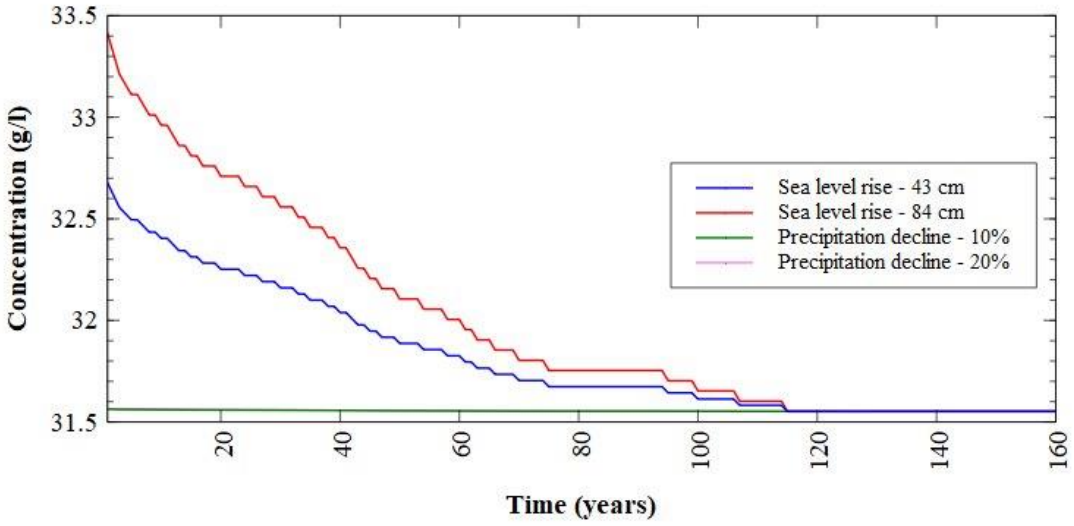

Figure 64 Change of concentration for piezometer P2 for mitigation measure M1 after climate changes

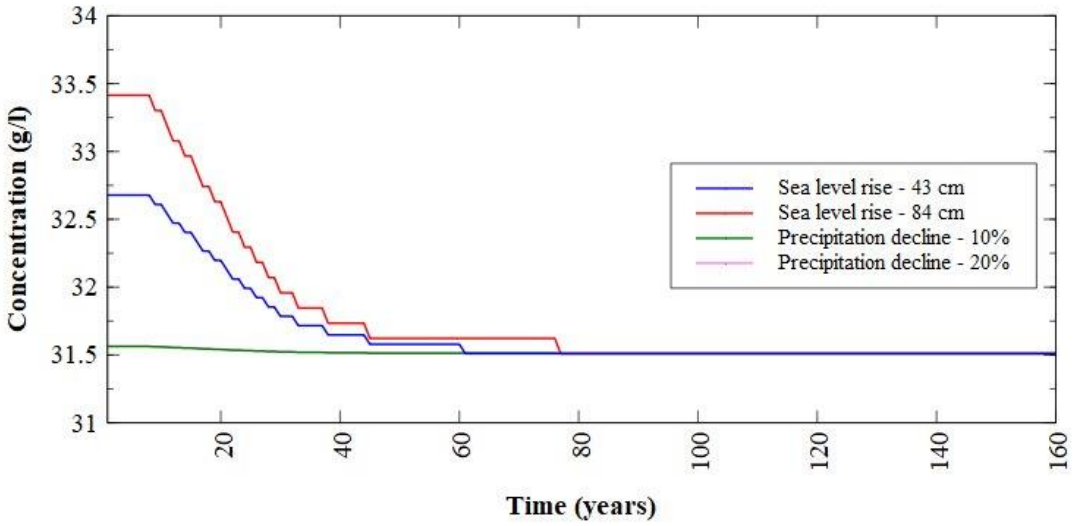

Figure 65 Change of concentration for piezometer P2 for mitigation measure M2 after climate changes

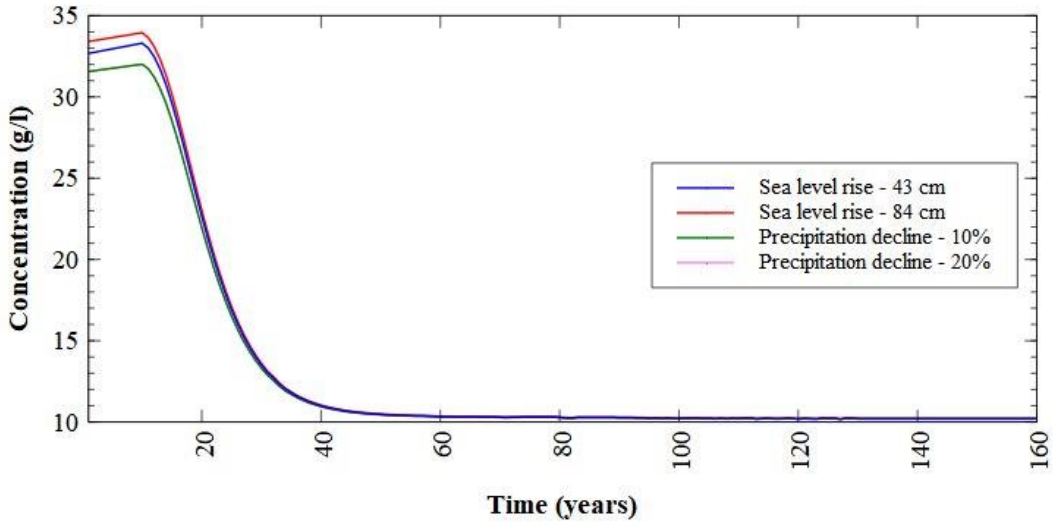

Figure 66 Change of concentration for piezometer P2 for mitigation measure M3 after climate changes

Table 4 Change of concentration and time needed to achieve steady state on location P2 for all mitigation measures after climate changes

		Mitigation measure M1	Mitigation measure M2	Mitigation measure M3
Change of concentration (g/l)	0.43 m SLR	-1.126	-1.168	-22.504
	0.84 m SLR	-1.862	-1.904	-23.227
	10% precipitation decline	-0.012	-0.053	-21.397
	20% precipitation decline	-0.015	-0.056	-21.400
Time needed to achieve steady state (years)	0.43 m SLR	115	60	130
	0.84 m SLR	120	76	132
	10% precipitation decline	38	33	50
	20% precipitation decline	40	34	51

Based on Figure 64 to Figure 66 it is possible to sea changes of concentration for location P2 for mitigation measures after climate changes. From the Table 4 it is possible to conclude that

mitigation measures M1 and M2 have very limited range in lowering concentration values. In both cases concentration value is reduced up to 2 g/l during the period of 120 years.

Mitigation measure M3 (barrier on River Neretva near Komin with channel parallel with River Neretva) shows best results and lowers concentration on the value around 10.2 g/l during the period of 132 years and the biggest drop in concentration values is during the first 50 years. Concentration on location P2 is lowered due to channel parallel with River Neretva that is a new source of fresh water in that area of the valley.

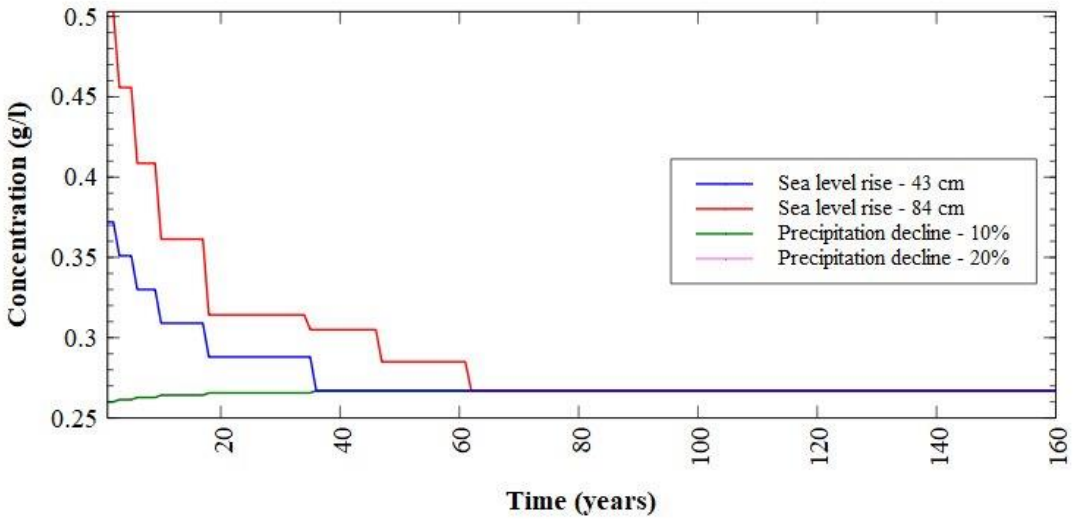

Figure 67 Change of concentration for piezometer P4 for mitigation measure M1 after climate changes

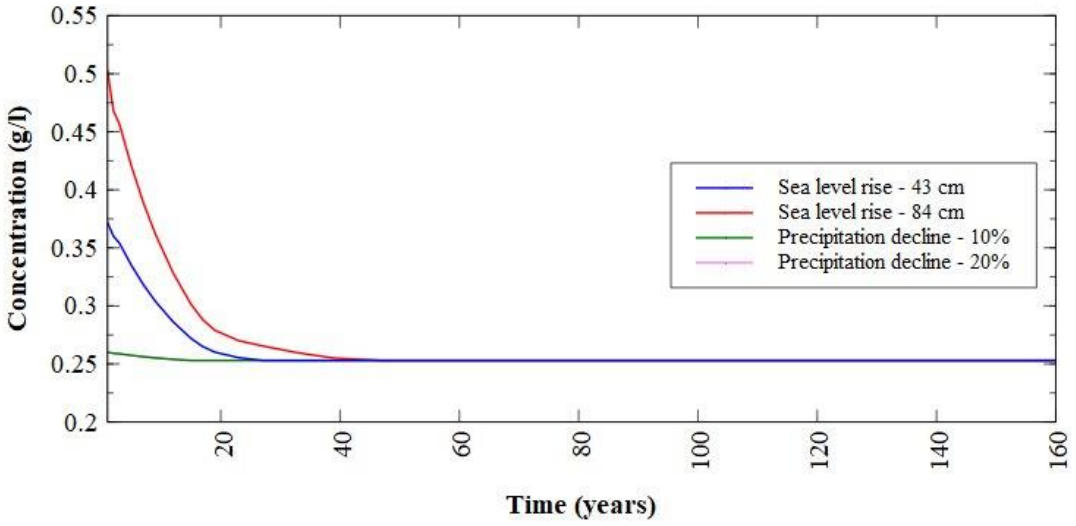

Figure 68 Change of concentration for piezometer P4 for mitigation measure M2 after climate changes

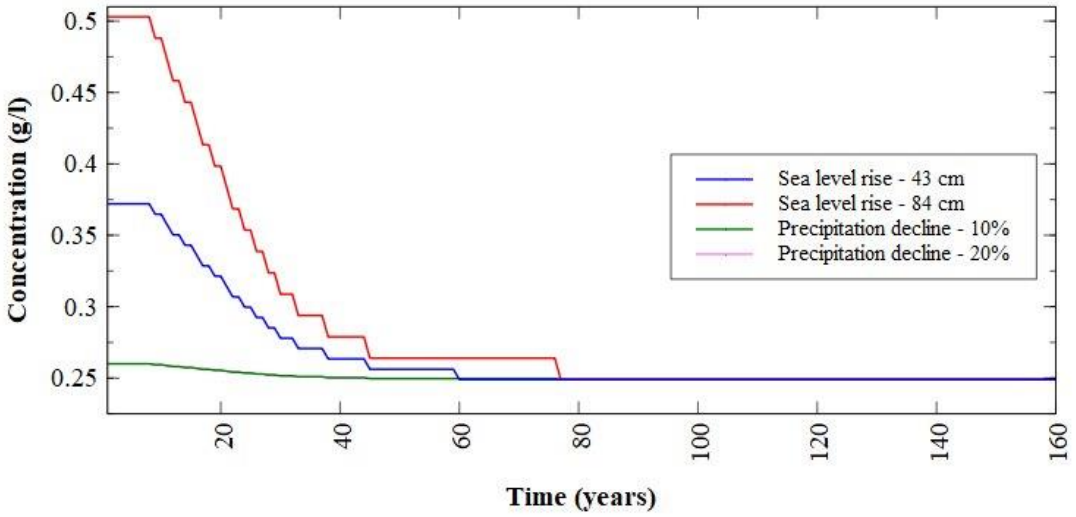

Figure 69 Change of concentration for piezometer P4 for mitigation measure M3 after climate changes

Table 5 Change of concentration and time needed to achieve steady state on location P4 for all mitigation measures after climate changes

		Mitigation measure M1	Mitigation measure M2	Mitigation measure M3
Change of concentration (g/l)	0.43 m SLR	-0.105	-0.119	-0.123
	0.84 m SLR	-0.236	-0.250	-0.254
	10% precipitation decline	-0.007	-0.007	-0.011
	20% precipitation decline	-0.007	-0.007	-0.011
Time needed to achieve steady state (years)	0.43 m SLR	36	27	60
	0.84 m SLR	62	46	77
	10% precipitation decline	36	15	45
	20% precipitation decline	36	15	45

On Figure 67 to Figure 69 and Table 5 it is possible to sea changes of concentration for location P4 for mitigation measures after climate changes. Since the location P4 is under greatest influence of River Mala Neretva, which is the source of fresh water during the whole year, local channels and pumping station Prag-Vidrice starting concentration values on location P4 are not high and all mitigation measures show similar results.

Bibliography

https://meteo.hr/klima.php?section=klima_modeli&param=klima_promjene. (s.d.).

https://www.eea.europa.eu/data-and-maps/figures/projected-changes-in-annual-and-5. (s.d.).

https://www.eea.europa.eu/ims/global-and-european-sea-level-rise. (s.d.).

https://www.ipcc.ch/srocc/chapter/chapter-4-sea-level-rise-and-implications-for-low-lying-islands-coasts-and-communities/. (s.d.).

List of figures

List of tables